be spectrally active under a site or a factor group model. Therefore this is an interesting example of a *non*-centrosymmetric molecule showing a centrosymmetric infrared and Raman mutually exclusive spectral pattern (Table II). Thus, the criterion for the detection of the factor group effects in this compound, where one expects it to be manifested as a separation between the infrared and Raman frequencies of the infrared–Raman coincident site group vibrational modes, cannot be used.

This investigation also confirms an earlier observation on the group 6B metal hexacarbonyls[18] by indicating the values of the derived polarizabilities perpendicular and parallel to the CO bond to be almost equal in magnitude but certainly opposite in sign.

Registry No. $Os_4O_4(CO)_{12}$, 29994-93-2.

Electron-Transfer Catalysis of Ligand Substitution in Triiron Clusters. The Role of the Bridging Ligand in Anion Radical Intermediates

H. H. Ohst and J. K. Kochi*

Contribution from the Department of Chemistry, University of Houston, University Park, Houston, Texas 77004. *Received October 10, 1985*

Abstract: The polynuclear cluster $Fe_3(CO)_9(\mu_3\text{-}PPh)_2$ (I) undergoes rapid ligand substitution by electron-transfer catalysis (ETC) under conditions in which the thermal process is nonexistent. X-ray crystallography and ^{31}P NMR spectroscopy establish the stepwise substitution of the CO ligands by trimethyl phosphite to take place selectively at three separate iron centers. The high selectivity to the mono-substitution product II is achieved by tuning the reduction potential specifically to generate catalytic amounts of the anion radical $Fe_3(CO)_9(PPh)_2^{-\cdot}$ ($I^{-\cdot}$) in either acetonitrile or tetrahydrofuran. Transient ESR spectroscopy of $I^{-\cdot}$ and three related paramagnetic intermediates establish the sequential transformation of anion radicals as they evolve in the ETC mechanism. The rate-limiting rearrangement of $I^{-\cdot}$ by the slippage of a phosphinidene cap from $\mu_3 \rightarrow \mu_2$ coordination underscores the key role of the bridging ligand in the substitution process. The importance of this critical transformation relates to the formation of a 17-electron, coordinatively unsaturated iron center in the otherwise intact cluster. As such, it emphasizes the key role that the bridging ligand can play in cluster activation.

Active interest in transition-metal clusters as catalysts derives from their conceptual relationship to catalytically active metal surfaces.[1,2] Indeed their delocalized electronic structure,[3] characteristic of metals, is reflected in their multiple redox behavior[4] as well as in their multimetal reactivity.[5] These two important aspects of catalytic activity may be coupled. Thus, if one considers that metal–metal bonding may not be stronger than metal–ligand bonding (except with the heaviest transition metals),[6] the polymetallic core should participate directly in the reactions of the clusters, especially under reducing conditions. For example, ESR studies have shown that the metal frameworks of trinuclear clusters with one and two μ_3-bridging ligands [i.e., $L_nM_3(\mu_3\text{-}E)$ and $L_mM_3(\mu_3\text{-}E)_2$ where E = CR, PR, or S] are weakened upon reduction, in accord with the metal–metal antibonding character of the LUMOs.[7-10] In these clusters, the bridging ligands E help to preserve the integrity of the cluster, since polynuclear metal carbonyls are known to otherwise undergo ready cleavage to species of lower nuclearity under reducing conditions.[11] Activation of metal clusters by reduction also relates to recent evidence that ligand substitutions of $L_nM_3(\mu_3\text{-}E)$[12] and $L_mM_3(\mu_3\text{-}E)_2$[13] are both strongly induced by electron attachment. Such studies of electron-transfer catalysis suggest that the chemical reactivity of metal clusters may generally be enhanced by deliberate reduction.[11-14]

We believe that electron-transfer catalysis (ETC) represents an important new method for cluster activation as it has proved to be for their mononuclear counterparts.[15] In this study, we examine the activation of the bicapped triiron cluster I to ligand substitution via labile radical anion intermediates. Most importantly, the ESR detection and characterization of a distinctive series of transient paramagnetic species provide an unusual opportunity to delineate the individual steps of the catalytic cycle involved in ETC.

(1) Moskovitz, M. *Acc. Chem. Res.* **1979**, *12*, 229.
(2) Muetterties, E. L.; Rhodin, R. N.; Band, E.; Brucker, C. F.; Pretzer, W. R. *Chem. Rev.* **1979**, *79*, 91.
(3) Wooley, R. G. In *Transition Metal Clusters*; Johnson, B. F. G., Ed.; Wiley: New York, 1980; p 607.
(4) See, e.g.: Vahrenkamp, H. *Adv. Organomet. Chem.* **1983**, *22*, 167.
(5) See: Deeming, A. J. In *Transition Metal Clusters*; Johnson, B. F. G., Ed.; Wiley: New York, 1980; p 391.
(6) Connor, J. A. In *Transition Metal Clusters*; Johnson, B. F. G., Ed.; Wiley: New York, 1980; p 345.
(7) (a) Strouse, C. E.; Dahl, L. F. *Discuss. Faraday Soc.* **1969**, *47*, 93. Stevenson, D. L.; Wei, C. H.; Dahl, L. F. *J. Am. Chem. Soc.* **1971**, *93*, 6027. Strouse, C. E.; Dahl, L. F. *J. Am. Chem. Soc.* **1971**, *93*, 6032. Frisch, P. D.; Dahl, L. F. *J. Am. Chem. Soc.* **1972**, *94*, 5082. (b) Beurich, H.; Madach, T.; Richter, F.; Vahrenkamp, H. *Agnew. Chem., Int. Ed. Engl.* **1979**, *18*, 690. (c) Bond, A. M.; Dawson, P. A.; Peake, B. M.; Rieger, P. H.; Robinson, B. H.; Simpson, J. *Inorg. Chem.* **1979**, *18*, 1413. (d) Peake, B. M.; Rieger, P. H.; Robinson, B. H.; Simpson, J. *Inorg. Chem.* **1981**, *20*, 2540. (e) Enoki, S.; Kawamura, T.; Yonezawa, T. *Inorg. Chem.* **1983**, *22*, 3821. (f) Kotz, J. C.; Petersen, J. V.; Reed, R. C. *J. Organomet. Chem.* **1976**, *120*, 433. (g) Bond, A. M.; Peake, B. M.; Robinson, B. H.; Simpson, J.; Watson, D. J. *Inorg. Chem.* **1977**, *16*, 410. (g) Lindsey, P. N.; Peake, B. M.; Robinson, B. H.; Simpson, J.; Honrath, U.; Vahrenkamp, H.; Bond, A. M. *Organometallics* **1984**, *3*, 413. (h) See also ref 17.
(8) Lindsey, P. N.; Peake, B. M.; Robinson, B. H.; Simpson, J.; Honrath, U.; Vahrenkamp, H.; Bond, A. M. *Organometallics* **1984**, *3*, 413.
(9) (a) Muller, M.; Vahrenkamp, H. *Chem. Ber.* **1983**, *116*, 2765. (b) Vahrenkamp, H. *Angew. Chem., Int. Ed. Engl.* **1979**, *18*, 690. (c) Honrath, U.; Shu-Tang, L.; Vahrenkamp, H. *Chem. Ber.* **1985**, *118*, 132.
(10) (a) Schilling, B. E. R.; Hoffmann, R. *J. Am. Chem. Soc.* **1979**, *101*, 3456. (b) Rives, A. B.; Xiao-Zeng, Y.; Fenske, R. F. *Inorg. Chem.* **1982**, *21*, 2286. (c) Chesky, P. T.; Hall, M. B. *Inorg. Chem.* **1983**, *22*, 2102. (d) Chesky, P. T.; Hall, M. B. *Inorg. Chem.* **1983**, *22*, 2998.
(11) (a) Vahrenkamp, H. *Struct. Bonding (Berlin)* **1977**, *32*, 1. (b) Deeming, A. J. In *Transition Metal Clusters*; Johnson, B. F. G., Ed.; Wiley: New York, 1980; Chapter 6.
(12) (a) Bezems, G. J.; Rieger, P. H.; Visco, S. *J. Chem. Soc., Chem. Commun.* **1981**, 265. (b) Bruce, M. I.; Kehoe, D. C.; Matisons, J. G.; Nicholson, B. K.; Rieger, P. H.; Williams, M. L. *J. Chem. Soc., Chem. Commun.* **1982**, 442.
(13) (a) Darchen, A.; Mahe, C.; Patin, H. *J. Chem. Soc., Chem. Commun.* **1982**, 243. (b) Darchen, A.; Mahe, C.; Patin, H. *Nouv. J. Chim.* **1982**, *6*, 539. (c) See also: Lhadi, E. K.; Mahe, C.; Patin, H.; Darchen, A. *J. Organomet. Chem.* **1983**, *246*, C61. And: Darchen, A.; Mahe, C.; Patin, H. *Nouv. J. Chim.* **1983**, *7*, 453.
(14) Arewgoda, M.; Robinson, B. H.; Simpson, J. *J. Am. Chem. Soc.* **1983**, *105*, 1893.
(15) Hershberger, J. W.; Kochi, J. K. *J. Chem. Soc., Chem. Commun.* **1982**, 212.

0002-7863/86/1508-2897$01.50/0

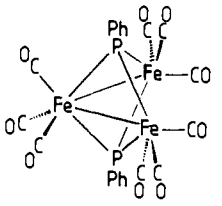

I

The catalytic process for $Fe_3(CO)_9(PPh)_2$ can be initiated both chemically and electrochemically. Thus, we wish to also show how electrochemical techniques, particularly cyclic voltammetry, are well-suited to study the facile and selective ligand substitution of metal clusters owing to electron-transfer rates which can be finely tuned to the electrode potential. Although the redox chemistry of μ_3-bridged clusters $L_nM_3(\mu_3\text{-}E)$ with a single cap has been established,[7-9,16,17] the electrochemistry of the bicapped clusters $L_mM_3(\mu_3\text{-}E)_2$ is less studied, with the exception of some clusters with E = μ_3-S.[7e,13,18] In this study, the choice of I with two phosphorus caps[19] provides an invaluable ESR probe (i.e., ^{31}P hyperfine splittings) with which to examine the role of the bridging ligand in the radical anion intermediates.

Results

Following the initial synthesis of the triiron cluster I, Treichel and co-workers[19] found that the thermal ligand substitution with trimethyl phosphite occurred rather slowly and unselectively.[20,21] Thus, a mixture of mono-, bis-, and tris-substitution products II, III, and IV, respectively, was formed in approximately equimolar amounts after refluxing a xylene solution for $5^1/_2$ h—and then only in low yields according to eq 1.

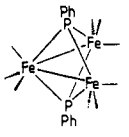

1

$$1 + nL \xrightarrow{[140\ ^\circ C]} \underset{\text{II-IV}}{Fe_3(CO)_{9-n}(PPh)_2L_n} + nCO \quad (1)$$

Electron-Transfer Catalysis of the Triiron Cluster I

We find that each substitution product can be *separately* synthesized at room temperature in good yields by simply passing a small cathodic current through the solution of the cluster. The ETC of ligand substitution was carried out in either acetonitrile or tetrahydrofuran (THF) containing supporting electrolyte at a constant potential E_p until 10–15% charge was consumed, as follows.

(1) The pure *monophosphite* substitution product II (n = 1) was isolated in 65% yield when the potential was maintained at E_p = –0.80 V vs. SCE, i.e., eq 2. Similarly when trimethyl

$$Fe_3(CO)_9(PPh)_2 + P(OMe)_3 \xrightarrow{[-0.80\ V]} \underset{\text{II}}{Fe_3(CO)_8(PPh)_2[P(OMe)_3]} + CO \quad (2)$$

phosphite was employed in place of triethylphosphine under the same conditions, the mono-substituted analogue V was obtained in 66% yield. The electrocatalytic nature of these substitution processes was readily deduced from the coulometry measured at constant current (see Table I). In the absence of such a cathodic current, the thermal substitution (eq 1) was too slow to observe.[19] When the reaction of I with trimethyl phosphite was carried out in the presence of a 10-fold excess of tri-*n*-butyltin hydride, no retardation of the rate or decrease in the yield of II was observed.[22]

(2) The pure bis-phosphite substitution product III (n = 2) was isolated in 63% yield, when a partial charge was first passed at E_p –0.80 V and then at –1.15 V, i.e., eq 3. Similarly the bis-substitution product VI was isolated in 66% yield when the added nucleophile was triethylphosphine.

$$Fe_3(CO)_9(PPh)_2 + 2P(OMe)_3 \xrightarrow{[-1.15\ V]} \underset{\text{III}}{Fe_3(CO)_7(PPh)_2[P(OMe)_3]_2} + 2CO \quad (3)$$

(3) The tris-phosphite IV (n = 3) can be obtained directly from I at E_p –1.40 V by a procedure similar to that described above, i.e., eq 4. However, we found that the best results were obtained

$$Fe_3(CO)_9(PPh)_2 + 3P(OMe)_3 \xrightarrow{[-1.40\ V]} \underset{\text{IV}}{Fe_3(CO)_6(PPh)_2[P(OMe)_3]_3} + 3CO \quad (4)$$

when the partially converted bis-phosphite III was employed as the reactant (see Table I). This modified procedure reflects the decreasing efficiency of the ligand substitution when three phosphites are introduced into the triiron cluster. In each case, optimum yields of 39% were obtained after reoxidation of the solution.

Electron-transfer catalysis of ligand substitution of I can also be induced chemically with small amounts of a reducing agent such as cobaltocene (E° = –0.95 V in acetonitrile).[23] For example, when I was treated with 0.08 equiv of cobaltocene in the presence of excess triethylphosphine in acetonitrile, the mono-substitution product V was isolated in 52% yield.

The facile ligand substitution of the triiron cluster I offers an excellent opportunity to examine the important facets of electron-transfer catalysis. We identify four key factors to be (A) the structures of the multiple substitution products, (B) the redox properties of the triiron clusters, (C) the nature of the anion radical intermediates, and (D) the kinetics of the catalytic substitution, which are discussed individually below.

A. Products and Stereochemistry of Ligand Substitution in Triiron Clusters. The successful isolation and growth of a single crystal of the tris-phosphite IV allowed its molecular structure to be established by X-ray crystallography. The selected bond lengths and bond angles for $Fe_3(CO)_6(PPh)_2[P(OMe)_3]_3$ (IV) are presented in Table II. The ORTEP diagram in Figure 1 shows $Fe_3(CO)_6(PPh)_2[(POMe)_3]_3$ to be structurally related to the

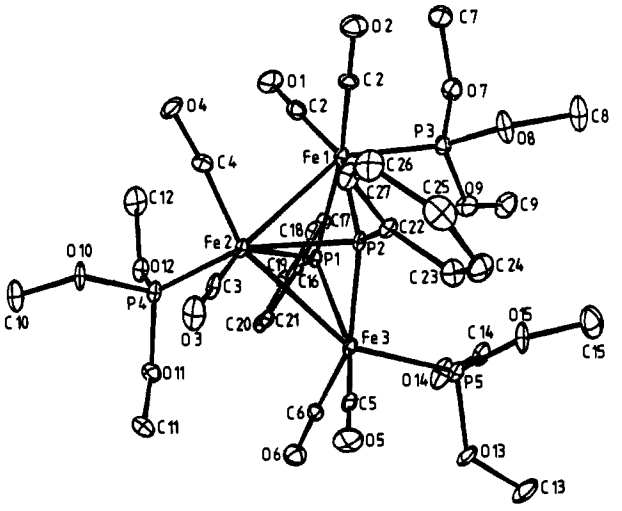

Figure 1. ORTEP diagram of the tris-phosphite $Fe_3(CO)_6(PPh)_2[P(OMe)_3]_3$ (IV) showing the location and stereochemistry of the phosphite ligands. The hydrogen atoms are omitted for clarity.

(16) (a) Peake, B. M.; Robinson, B. H.; Simpson, J.; Watson, D. J. *Inorg. Chem.* **1977**, *16*, 405. (b) Bond, A. M.; Dawson, P.; Peake, B. M.; Robinson, B. H.; Simpson, J. *Inorg. Chem.* **1979**, *18*, 1413. (c) See also ref 7d.

(17) Honrath, U.; Vahrenkamp, H. *Z. Naturforsch, B* **1984**, *39b*, 555.

(18) Madach, T.; Vahrenkamp, H. *Chem. Ber.* **1981**, *114*, 505.

(19) Treichel, P. M.; Dean, W. K.; Douglas, W. M. *Inorg. Chem.* **1972**, *11*, 1609.

(20) See also: Kouba, J. K.; Muetterties, E. L.; Thompson, M. R.; Day, V. W. *Organometallics* **1983**, *2*, 1065. And ref 21.

(21) (a) Vahrenkamp, H.; Wucherer, E. J.; Wolters, D. *Chem. Ber.* **1983**, *116*, 1219. (b) Lang et al. (Lang, H.; Zsolnai, L.; Huttner, G. *J. Organomet. Chem.* **1985**, *282*, 23) showed the low thermal reactivity of the triiron cluster I.

(22) Thus, reactions at the coordinated CO ligand in the anion radical such as hydrogen atom transfer is not a factor. See: Narayanan, B. A.; Kochi, J. K. *J. Organomet. Chem.* **1984**, *272*, C49.

(23) Koelle, U. *J. Organomet. Chem.* **1978**, *152*, 225.

Table I. Electrocatalytic Synthesis of Triiron Cluster Derivatives[a]

triiron cluster reactant	solvent	added ligand	potential, V	electron consumed[b]	product	isolated yield, %
$Fe_3(CO)_9(PPh)_2$	THF	$P(OMe)_3$	−0.80	0.05	$Fe_3(CO)_8(PPh)_2[P(OMe)_3]$	65
$Fe_3(CO)_9(PPh)_2$	THF	$P(OMe)_3$	−0.80	0.1		
			-1.15	0.1	$Fe_3(CO)_7(PPh)_2[P(OMe)_3]_2$	63
$Fe_3(CO)_9(PPh)_2$	CH_3CN	$P(OMe)_3$	−0.80	0.1		
			-1.15	0.1	$Fe_3(CO)_7(PPh)_2[P(OMe)_3]_2$	62
$Fe_3(CO)_7(PPh)_2[P(OMe)_3]_2$	CH_3CN	$P(OMe)_3$	-1.40	1.0	$Fe_3(CO)_6(PPh)_2[P(OMe)_3]_3$	39
$Fe_3(CO)_9(PPh)_2$	THF	PEt_3	−0.80	0.1	$Fe_3(CO)_8(PPh)_2[PEt_3]$	66
$Fe_3(CO)_9(PPh)_2$	CH_3CN	PEt_3	−0.80	0.1		
			−1.15	0.1	$Fe_3(CO)_7(PPh)_2[PEt_3]_2$	58

[a] In 25 mL of solvent containing 0.3 mmol of triiron cluster, 17 mmol of added ligand, and 0.3 M tetrabutylammonium perchlorate at 25 °C. [b] Total faradays of charge passed relative to triiron clusters.

Table II. Selected Bond Lengths and Bond Angles in $Fe_3(CO)_6(PPh)_2[P(OMe)_3]_3$ (**IV**)

bond lengths, Å			bond angles, deg			
A	B		A	B	C	
Fe(1)	Fe(2)	2.681 (1)	Fe(1)	Fe(2)	Fe(3)	83.93 (2)
Fe(2)	Fe(3)	2.736 (1)	Fe(1)	P(1)	Fe(3)	108.31 (4)
Fe(1)	P(1)	2.234 (1)	Fe(1)	P(2)	Fe(3)	109.52 (4)
Fe(1)	P(2)	2.222 (1)	P(1)	Fe(1)	P(2)	70.29 (4)
Fe(2)	P(1)	2.242 (1)	P(1)	Fe(3)	P(2)	70.47 (4)
Fe(2)	P(2)	2.252 (1)	P(1)	Fe(1)	P(3)	98.41 (4)
Fe(3)	P(1)	2.234 (1)	P(2)	Fe(1)	P(3)	101.54 (4)
Fe(3)	P(2)	2.213 (1)	P(1)	Fe(3)	P(5)	107.24 (4)
Fe(1)	P(3)	2.133 (1)	P(2)	Fe(3)	P(5)	104.83 (4)
Fe(2)	P(4)	2.150 (1)				
Fe(3)	P(5)	2.142 (1)				
Fe(1)	Fe(3)	3.622 (1)				
P(1)	P(2)	2.566 (1)				

precursor I by successive substitution at the three separate iron centers. Stereochemically, the pair of phosphites on Fe(1) and Fe(3) are equivalent—both occupying axial positions (as defined by Muetterties et al.[20]). The unique phosphite ligand on the Fe(2) lies above an iron–phosphorus bond in a staggered position. Most significantly, the bond distances and the bond angles in the Fe_3P_2 core are essentially the same (Table II) as those previously found in the parent I.[24] Thus, the Fe(1)–Fe(2) and Fe(2)–Fe(3) distances of 2.681 and 2.736 Å, respectively, represent single bonds, whereas the Fe(1)–Fe(3) bond length of 3.622 Å precludes any bonding interaction between these extreme centers. Aside from phosphite substitutions, the principal difference between I and IV is a conformational one—the torsional angle of the two phenyl rings increases from ~0° in I to 80° in IV, probably as a result of the nonbonded interactions with the phosphite ligands.

The establishment of the molecular structure of the tris-phosphite IV permits the structural assignment of the mono and bis derivatives from their ^{31}P NMR spectra in solution (Table III). Thus, the low-temperature (−77 °C) NMR spectrum of IV in toluene consists of a pair of triplets at δ 268 and 181 and a singlet at δ 184 (in a 2:2:1 intensity ratio), arising from the two phosphinidene caps, the two axial phosphites P_1 at the basal Fe(1) and Fe(3), and the unique phosphite P_2 on the apical Fe(2),[25] respectively, in structure IVa represented schematically in eq 5. At

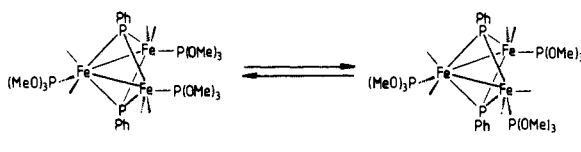

IVa IVb (5)

−5 °C, the triplet resonance of the tris-phosphite derivative IV at δ 181 collapses to re-form a broadened singlet at 67 °C owing to the fluxionality of the basal phosphites P_1.[26] The ready interconversion of axial and equatorial conformations is also shown in the low-temperature ^{31}P NMR spectrum by the presence of isomer IVb (see Table III) in minor amounts.[27]

The low-temperature ^{31}P NMR spectrum of the mono-phosphite II in Table III is consistent with structure IIa, in which $P(OMe)_3$ adopts the axial conformation on the basal Fe(1), i.e., eq 6, as also reported earlier by Muetterties and co-workers.[28] The

IIa IIb (6)

mono-triethylphosphine derivative V is assigned a structure analogous to IIa on the basis of a similar ^{31}P NMR spectrum. The mono-phosphite IIa undergoes a slow thermal (basal → apical) rearrangement upon standing at room temperature for a week. The structure of the isomeric IIb is readily deduced from the ^{31}P NMR spectrum showing a pair of 2:1 singlets at δ 317 and 183 for the phosphinidene caps and the apical phosphite, respectively.[29,30]

The bis-phosphite III consists of a mixture of two isomers IIIa and IIIb, in which substitution has occurred at Fe(1)–Fe(2) and Fe(1)–Fe(3), respectively (eq 7). The structural assignments of

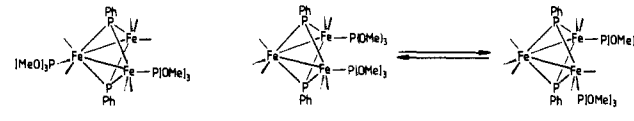

IIIa IIIb IIIc (7)

IIIa and IIIb are readily deduced by interpolation from the ^{31}P spectra of the mono- and tris-phosphite analogues.[32] Thus, the ^{31}P NMR spectrum of IIIa consists of a doublet (δ 299), triplet (δ 184), and singlet (δ 187) in a 2:1:1 intensity ratio for the phosphinidene caps, the basal phosphite P_1, and the apical phosphite P_2,[28] respectively. The isomeric IIIb on the other hand shows a pair of triplets (δ 265, 185) in a 2:2 intensity ratio for the pair of equivalent phosphites in axial conformations on Fe(1)–Fe(3). The latter undergo fluxional axial ⇄ equatorial interconversions in a manner similar to that described for IVa ⇄

(24) (a) Cook, S. L.; Evans, J.; Gray, L. R.; Webster, M. *J. Organomet. Chem.* **1982**, *236*, 367. (b) Compare also the structure of the bis-acetonitrile derivative $Fe_3(CO)_7(PPh)_2(NCMe)_2$.[20]

(25) The small, unresolved coupling of the apical phosphite and the phosphinidene caps is also shown in IIb and IIIa.

(26) For the temperature-dependent line broadening in the NMR spectra which is characteristic of such fluxional behavior, see ref 20.

(27) Integration indicates the relative amounts of IVa and IVb to be 95:5.

(28) The fluxional interconversion of $P(OMe)_3$ between axial ⇄ equatorial conformers of IIa is described in ref 20, See also: Aime, S.; Milone, L.; Rossetti, R.; Stanghellini, P. L. *J. Chem. Soc., Dalton Trans.* **1980**, 46.

(29) Note also the small, unresolved coupling between the apical phosphite ligand and the phosphinidene caps in IIIa and IVa.

(30) Such an isomerization can occur via a shift of Fe–Fe bonds without the cleavage of the Fe(1)–$P(OMe)_3$ bond. Thus, the isostructural triosmium cluster[31] undergoes reversible formation and cleavage of Os–Os bonds leading to the exchange of cluster positions.

(31) Süss-Fink, G.; Thewalt, U.; Klein, H.-P. *J. Organomet. Chem.* **1982**, *224*, 59.

(32) The geminally disubstituted 1,1-isomer exhibits different ^{31}P NMR and IR spectra.[20]

Table III. ^{31}P NMR Spectra of the Triiron Clusters[a]

				chemical shift δ ^{31}P $\{^1H\}$ (J, Hz)			
					ligand		
	triiron cluster	temp, °C	isomer	μ_3-PPh	1	2	3
II	$Fe_3(CO)_8(PPh)_2[P(OMe)_3]$	-64	IIa	299.1 (d, 46)	182.0 (t, 46)		
		25	IIb	317.0 (s)	183.4 (s)		
III	$Fe_3(CO)_7(PPh)_2[P(OMe)_3]_2$	-66	IIIa	299.0 (d, 39)	184.1 (t, 39)	186.8 (s)	
		-66	IIIb	264.7 (t, 39)	185.4 (t, 39)		
		-66	IIIc	315.6, 287.5, (AB, 289)	184.0 (t, 39)	173.2 (dd, 96, 62)	
IV	$Fe_3(CO)_6(PPh)_2[P(OMe)_3]_3$	-77[b]	IVa	268.5 (t, 39)	181.4 (t, 39)	183.9 (s)	
		-77[b]	IVb	296.1, 290.5 (AB, 299)	181.4 (t, 39)	165.0 (dd, 73, 49)	183.9 (s)
V	$Fe_3(CO)_8(PPh)_2[PEt_3]$	-52	Va	283.7 (d, 39)	60.9 (t, 39)		
		25	Vb	312.0 (s)	49.2 (s)		
VI	$Fe_3(CO)_7(PPh)_2[PEt_3]_2$	-64	Vb	282.0 (d, 34)	56.3 (t, 34)	48.4 (s)	

[a] In $CDCl_3$, unless indicated otherwise. [b] In C_7D_8.

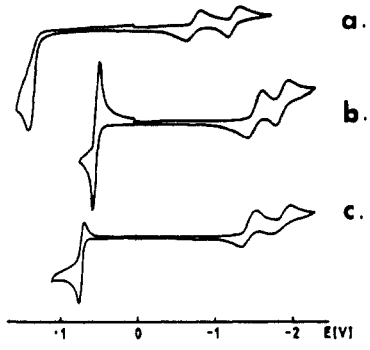

Figure 2. Initial cathodic scan cyclic voltammograms of (a) 3.3×10^{-3} M $Fe_3(CO)_9(PPh)_2$, (b) 6.7×10^{-4} M $Fe_3(CO)_6(PPh)_2[P(OMe)_3]_3$, and (c) 1.8×10^{-3} M $Fe_3(CO)_7(PPh)_2[PEt_3]_2$ in THF containing 0.3 M TBAP at 100 mV s^{-1} at 25 °C.

IVb, as shown by the temperature-dependent line broadening of the low-temperature ^{31}P NMR spectrum of IIIc (Table III).[33]

B. Redox Properties of the Triiron Clusters. The preparative synthesis of each triiron cluster (II–IV) is controlled by the potential E_p, which determines the selectivity in ligand substitution by selecting the particular triiron carbonyl to be reduced to its labile radical anion. The reduction of the triiron clusters can be examined individually by both electrochemical and chemical methods, as described below.

(1) The *electrochemical reduction* of the triiron carbonyl I is best considered from the cyclic voltammogram (CV) in Figure 2, which shows a pair of one-electron reversible waves with the first cathodic maximum at E_p^c −0.79 V. [A third reduction wave (E_p^c −2.69 V, not shown) is irreversible, as is the anodic wave (E_p^c 1.37 V) which consumes more than three electrons by coulometry.] The bulk electroreduction of I at the potential (−0.80 V) of the first CV wave consumes one electron and leads to a dark-green solution of $I^{-}\cdot$ in either tetrahydrofuran (THF), methylene chloride, or acetonitrile as the solvent,[34] i.e., eq 8. The infrared spectrum

$$\underset{\text{I}}{Fe_3(CO)_9(PPh)_2} + e \overset{E^0}{\rightleftharpoons} \underset{\text{I}^{-}\cdot}{Fe_3(CO)_9(PPh)_2^{-}\cdot} \qquad (8)$$

of the monoanion $Fe_3(CO)_9(PPh)_2^{-}\cdot$ is typically shown in Figure 3a, in comparison with that of the parent cluster I. The second reversible CV wave at E^0 −1.30 V corresponds to the formation of the red-brown diamagnetic dianion $Fe_3(CO)_9(PPh)_2^{2-}$ (which will be elaborated separately[35]).

The stepwise substitution of the carbonyls in the parent triiron cluster I by ligands with greater donor properties, such as trimethyl phosphite (n = 1–3) and triethylphosphine (n = 1, 2), is reflected in a shift of E_p^c (or E^0)[36] to successively more negative potentials

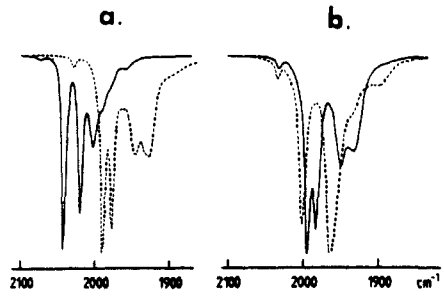

Figure 3. Infrared spectra of triiron clusters. (a) $Fe_3(CO)_9(PPh)_2$ (I) (—) and $Fe_3(CO)_9(PPh)_2^{-}\cdot$ ($I^{-}\cdot$) (---) in THF. (b) $I^{-}\cdot$ (—) and $I'^{-}\cdot$ (---) in MeCN.

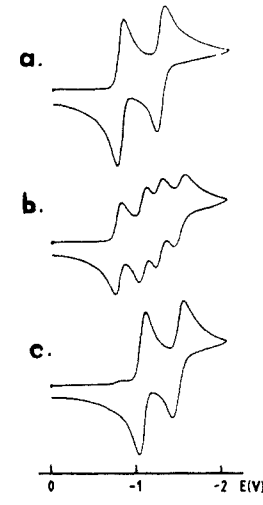

Figure 4. Initial cathodic scan cyclic voltammograms at 100 mV s^{-1} and 25 °C of 5.8×10^{-3} M $Fe_3(CO)_9(PPh)_2$ in THF containing 0.3 M TBAP and 0.16 M $P(OMe)_3$: (a) after passing 10% cathodic current, (b) 33 min later, and (c) 77 min later. Note (b) is a composite of (a) and (c).

(Table II). Nonetheless, the chemically reversible character of the first two reduction waves is maintained throughout the series of substituted triiron clusters II–VI. It is important to note that the cathodic potential E_p^c which characterizes each substitution product is precisely that required to attain selectivity in the preparative procedures described above. For example, consider the cyclic voltammogram of I in the presence of $P(OMe)_3$ in Figure 4a which shows essentially no difference from that in Figure 2. The cyclic voltammogram in Figure 4c represents the clean conversion to the mono-phosphite II upon the passage of a small (10%) cathodic current at −0.80 V. Similar results are obtained in bis substitution and tris substitution, as shown by a comparison of the electrode potentials in Table I with the values of E_p^c required to reduce II and III, respectively (Table IV).

(33) For the relative populations of IIIa, IIIb, and IIIc, see discussion in Experimental Section.

(34) With tetra-*n*-butylammonium perchlorate (TBAP) as the supporting electrolyte, 0.3 M in THF, 0.1 M in MeCN, and 0.1 M in CH_2Cl_2.

(35) (a) For a preliminary report, see: Ohst, H. H.; Kochi, J. K. *J. Chem. Soc., Chem. Commun.* **1986**, 121. (b) Ohst, H. H.; Kochi, J. K. *Inorg. Chem.*, in press.

(36) In a chemically reversible system, $E^0 \cong {}^1/_2(E_p^c + E_p^a)$; see footnote 6 in: Howell, J. L.; Goncalves, J. M.; Amatore, C.; Klasinc, L.; Wightman, R. M.; Kochi, J. K. *J. Am. Chem. Soc.* **1984**, *106*, 3968.

Table IV. Redox Potentials of Triiron Clusters[a]

	triiron cluster	reduction $E_{1/2}(1)$	reduction $E_{1/2}(2)$	oxidation E_p	oxidation $E_{1/2}$
I	$Fe_3(CO)_9(\mu_3\text{-}PPh)_2$	−0.79	−1.30[b]	+1.37	
II	$Fe_3(CO)_8(\mu_3\text{-}PPh)_2[P(OMe)_3]$	-1.09	-1.54	+1.18	
III	$Fe_3(CO)_7(\mu_3\text{-}PPh)_2[P(OMe)_3]_2$	-1.32	-1.68	+1.12	
				+0.80	+0.72[c]
IV	$Fe_3(CO)_6(\mu_3\text{-}PPh)_2[P(OMe)_3]_3$	−1.52	−1.88		+0.49
V	$Fe_3(CO)_8(\mu_3\text{-}PPh)_2(PEt_3)$	-1.16	-1.64	+1.05	
VI	$Fe_3(CO)_7(\mu_3\text{-}PPh)_2(PEt_3)_2$	-1.44	-1.85		+0.71

[a] From the cyclic voltammetry of 10^{-3} M triiron cluster in THF containing 0.3 M TBAP at 100 mV s^{-1} and 25 °C. Potentials in volts vs. SCE. $E_{1/2}$ are reversible potentials. E_p are irreversible peak potentials measured at 100 mV s^{-1}. [b] Third irreversible wave at E_p = −2.69 V. [c] At -50 °C.

The cyclic voltammetric studies thus underscore the strong influence of phosphite and phosphine ligands on the reduction potential of the triiron cluster. Such an electronic effect derives from their properties as donor ligands which raise the energy level of the cluster LUMO.[37] By the same reasoning, the presence of donor ligands facilitates the oxidation of triiron clusters in like measure. Thus, the irreversible anodic wave of I at E_p^a 1.37 V is shifted to 1.18 V in the mono-phosphite II, to 0.80 V in the bis-phosphite III, and to 0.50 V in the tris-phosphite IV with a concomitant enhancement in the reversibility of the CV wave. For example, the anodic CV wave of III becomes chemically reversible as the temperature is lowered to −50 °C. By contrast, the corresponding CV wave of the tris-phosphite IV is reversible even at room temperature. The comparatively better donor property of triethylphosphine relative to trimethyl phosphite is shown by the more negative values of E_p^a in the mono and bis derivatives. Furthermore, two triethylphosphine ligands are sufficient to confer reversibility to the CV waves, as in VI. In these triiron clusters, the increasing reversibility of the CV wave relates to increasing persistence of the cation radical.[38]

(2) The *chemical reduction* of the triiron cluster I to the anion radical was effected either with 1 equiv of sodionaphthalene or by 1% sodioamalgam in tetrahydrofuran. The infrared spectrum of $Fe_3(CO)_9(PPh)_2^{-\cdot}$ obtained with these reducing agents was identical with that generated electrochemically (Figure 3a). The reduction of I with cobaltocene was complete in THF only by employing a large excess of the reducing agent. However, the reduction occurs rapidly and quantitatively with stoichiometric amounts of cobaltocene when it was carried out in acetonitrile. Thus, when acetonitrile solutions of I and cobaltocene were mixed at −40 °C, a dark-green solution was formed immediately, indicating the rapid redox reaction produced the anion radical $Fe_3(CO)_9(PPh)_2^{-\cdot}$, i.e., eq 9, as also established by an inspection

$$Fe_3(CO)_9(PPh)_2 + Cp_2Co \rightarrow Fe_3(CO)_9(PPh)_2^{-\cdot} + Cp_2Co^+ \quad (9)$$

of the IR spectrum of the resultant solution. Repeated attempts to isolate a single crystal of $Fe_3(CO)_9(PPh)_2^{-\cdot}$ were unsuccessful. However, the structure of the anion radical $I^{-\cdot}$ is elucidated from its ESR spectrum, described below.

C. ESR Studies of Triiron Cluster Anion Radicals as Reaction Intermediates. Electron spin resonance (ESR) spectroscopy provides the most direct means to examine the structure and chemical behavior of the anion radicals of the triiron clusters, particularly the transient species.[39] The isotropic ESR spectrum obtained from the one-electron reduction of the parent cluster I by cobaltocene in acetonitrile is shown in Figure 5a. It clearly

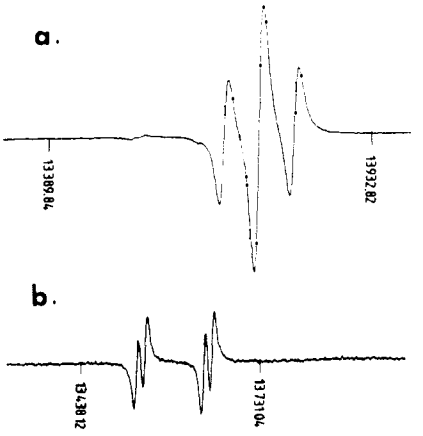

Figure 5. ESR spectra (X-band) of anion radicals in MeCN derived by (a) reduction of $Fe_3(CO)_9(PPh)_2$ (I) with Cp_2Co to $I^{-\cdot}$ and (b) rearrangement of $I^{-\cdot}$ to $I'^{-\cdot}$ after standing 8 h. Proton NMR field markers are in kilohertz.

Table V. ESR Parameters of Open Anion Radicals $Fe_3(CO)_8(\mu_3\text{-}PPh)(\mu_2\text{-}PPh)L^{-\cdot}$[a]

L	$\langle g \rangle$	^{31}P hyperfine splitting, G μ_3-P	μ_2-P	L
CO	2.039	25.3 (d)	3.4 (d)	
$P(OMe)_3$	2.041	25.3 (d)	3.4 (d)	25.3 (d)
PPh_3	2.040	25.5 (d)	3.4 (d)	18.8 (d)
PEt_3	2.041	24.8 (d)	3.4 (d)	20.3 (d)
$P(OPh)_3$	2.040	25.8 (d)	3.8 (d)	23.1 (d)

[a] Spectra recorded in acetonitrile at 25 °C by (a) reduction of $Fe_3(CO)_8(PPh)_2L$ with cobaltocene or (b) reaction of $Fe_3(CO)_9(\mu_3\text{-}PPh)(\mu_2\text{-}PPh)^{-\cdot}$ with ligand L.

Table VI. ESR Parameters of Closed Anion Radicals $Fe_3(CO)_8(\mu_3\text{-}PPh)^{-\cdot}$[a]

triiron cluster anion radical	$\langle g \rangle$	^{31}P hyperfine splitting, G μ_3-P	L
$Fe_3(CO)_9(\mu_3\text{-}PPh)_2^{-\cdot}$	2.019[b]	13.3 (t)	
$Fe_3(CO)_8(\mu_3\text{-}PPh)_2[PEt_3]^{-\cdot}$	2.027	18.3 (t)	18.3 (d)
$Fe_3(cO)_8(\mu_3\text{-}PPh)_2[P(OMe)_3]^-$	2.023	17.8 (t)	36.0 (d)
$Fe_3(CO)_8(\mu_3\text{-}PPh)_2[PPh_3)^{-\cdot}$	2.021	17.5 (t)	79.5 (d)

[a] In THF solution at 25 °C by (i) the reaction of $Fe_3(CO)_9(\mu_3\text{-}PPh)_2^{-\cdot}$ with ligand or (ii) the reduction of $Fe_3(CO)_8(PPh)_2L$ with sodium amalgam. [b] Same spectrum obtained in MeCN by reduction with cobaltocene.

consists of a simple 1:2:1 triplet at $\langle g \rangle$ = 2.019 with a hyperfine splitting a_p of 13.3 G, which arises from two equivalent phosphinidene caps in the symmetrical anion radical $I^{-\cdot}$, i.e., eq 10.

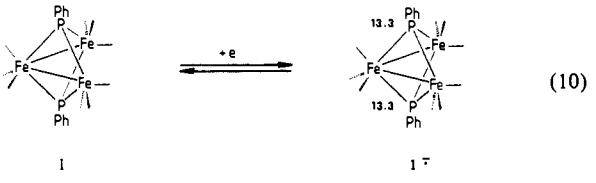

I $I^{-\cdot}$ (10)

The minimal structural change attendant upon such a simple electron accession to the parent triiron cluster is indicated by the similarity of the infrared spectrum of $I^{-\cdot}$ with that of I in the carbonyl region between 1900 and 2100 cm^{-1} (except for a shift) in Figure 3a.[40] Upon standing, this species is converted to a different anion radical $I'^{-\cdot}$ within a few hours, as indicated by the appearance of a new ESR spectrum (Figure 5b) consisting of a doublet of doublets at $\langle g \rangle$ = 2.039 with hyperfine splittings of 25.3 and 3.4 G from a pair of inequivalent phosphinidene caps. The rather deep-seated structural change accompanying the

(37) (a) Cf.: Madach, T.; Vahrenkamp, H. *Chem. Ber.* **1981**, *114*, 513. (b) See: Richmond, M. G.; Kochi, J. K. *Inorg. Chem.*, in press.

(38) For a discussion of this point, see related papers to: Klingler, R. J.; Kochi, J. K. *J. Am. Chem. Soc.* **1980**, *102*, 4790.

(39) For ESR studies of the anion radicals of various iron carbonyls, see: (a) Dawson, P. A.; Peake, B. M.; Robinson, B. H.; Simpson, J. *Inorg. Chem.* **1980**, *19*, 465. (b) Krusic, P. J.; San Filippo, J., Jr.; Hutchinson, B.; Hance, R. L.; Daniels, L. M. *J. Am. Chem. Soc.* **1981**, *103*, 2129. (c) Peake, B. M.; Robinson, B. H.; Simpson, J.; Watson, D. J. *J. Chem. Soc., Chem. Commun.* **1974**, 945. Miholova, D.; Klima, J.; Vleck, A. A.; *Inorg. Chim. Acta* **1978**, *27*, L67.

(40) A similar relationship between IR spectra and structure has been discussed in ref 16a.

conversion $I^- \rightarrow I'^{-\cdot}$ is also shown by a corresponding alteration of the infrared spectrum in a significant way (see Figure 3b).[41] Such a desymmetrization of the anion radical is most readily formulated as a conversion of one of the μ_3-phosphinidene caps to a μ_2-bridge by scission of a bond to iron, e.g., eq 11. [The

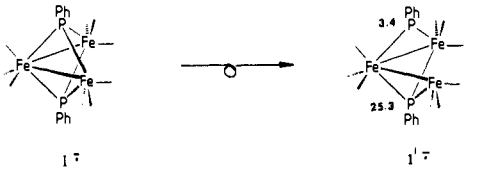

(11)

$I^{-\cdot}$ $I'^{-\cdot}$

ESR spectra of the anion radicals of the phosphine (L) derivatives $Fe_3(CO)_8(PPh)_2L$ provide the most definitive information (see Tables V and VI) about this structural change.[42]]

When the unsymmetrical anion radical $I'^{-\cdot}$ is treated with a ligand L such as trimethyl phosphite, it is immediately converted to the anion radical $II'^{-\cdot}$ of the substitution product with loss of carbon monoxide (eq 12). The ESR spectra of $II'^{-\cdot}$ derived from

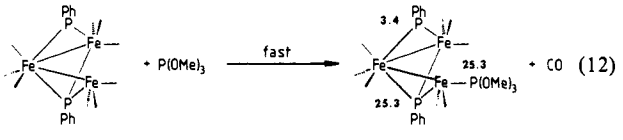

(12)

$I'^{-\cdot}$ $II'^{-\cdot}$

three representative phosphines and phosphites are shown in Figure 6 to illustrate the various phosphorus splittings associated with such cluster anion radicals. In each case, the hyperfine splitting pattern consists of three doublets (Table V), two of which remain relatively constant at $a_p \sim 25$ and 3.5 G. Since these are the same as those observed in the open parent $I'^{-\cdot}$, we consider them to be diagnostic of the μ_3-PPh and μ_2-PPh caps. The third doublet $a_P(L)$ varies systematically with structural changes of the phosphorus ligand as shown in column 5, Table V. Indeed the magnitudes of these phosphorus hyperfine splittings in the anion radicals $II'^{-\cdot}$ are strikingly akin to those previously observed in $Fe(CO)_3L_2^+$ by Connelly et al.[43] Such a relationship of $a_P(L)$ together with $\langle g \rangle$ values which are similar for $II'^{-\cdot}$ and $Fe(CO)_3L_2^+$ supports the open structure with a 17-electron iron center for the clusters $I'^{-\cdot}$ and $II'^{-\cdot}$ as depicted in eq 11 and 12, respectively.

Similarly, when the parent anion radical $I^{-\cdot}$ is treated with trimethyl phosphite in acetonitrile, the ESR spectrum gradually changed from that of $I^{-\cdot}$ to that of $II'^{-\cdot}$, i.e., eq 13. Although

(13)

$I^{-\cdot}$ $II'^{-\cdot}$

the ESR spectrum of $I'^{-\cdot}$ is not apparent during this conversion, it is likely to be an intermediate in eq 13. Thus, the rate of eq 13 is comparable to the rate of the rearrangement in eq 11, and both are significantly slower than the rate of ligand substitution in eq 12. Accordingly, we conclude the sequence of events in eq 13 to be as in eq 14.

$$I^{-\cdot} \xrightarrow{\text{slow}} I'^{-\cdot} \xrightarrow[P(OMe)_3]{\text{fast}} II'^{-\cdot} + CO \qquad (14)$$

Solvent polarity plays an important role with triiron anion radicals. For example, when $I^{-\cdot}$ is generated in tetrahydrofuran, it shows no tendency to rearrange to the unsymmetrical $I'^{-\cdot}$, even upon heating the solution. [Note that the ESR spectrum of $I^{-\cdot}$ in tetrahydrofuran (Figure 7a) is the same as that obtained in acetonitrile (see Figure 5a), and it remains unchanged in this solvent.] The addition of trimethyl phosphite to $I^{-\cdot}$ in tetrahydrofuran caused it to evolve into a new species $II^{-\cdot}$ whose ESR spectrum consists of a triplet (a_P = 17.8 G) of doublets (a_P = 36.0

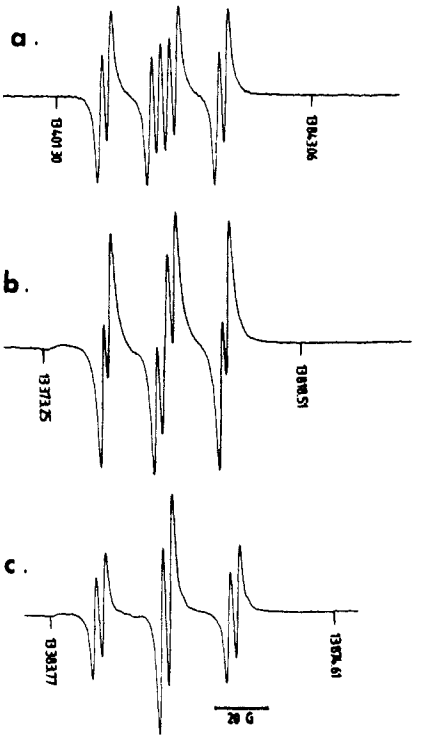

Figure 6. ESR spectra of open anion radicals $II'^{-\cdot}$ $Fe_3(CO)_8(\mu_3\text{-}PPh)(\mu_2\text{-}PPh)L^{-\cdot}$ with L (a) triphenylphosphine, (b) triethylphosphine, and (c) trimethyl phosphite in acetonitrile at 25 °C. Proton NMR field markers are in kilohertz.

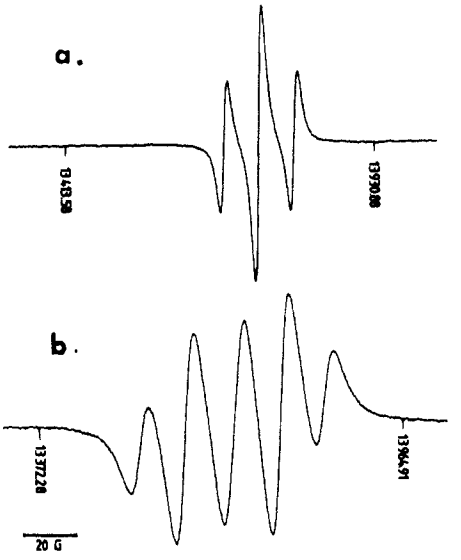

Figure 7. ESR spectra of triiron anion radicals in THF: (a) $I^{-\cdot}$ from reduction with 1% sodioamalgam and (b) $II^{-\cdot}$ by treatment of (a) with $P(OMe)_3$ at 25 °C.

(41) The IR spectrum of $I'^{-\cdot}$ bears a strong relationship to the IR spectrum of the open structure in $Fe_3(CO)_9(\mu_3\text{-}PPh)(\mu_2\text{-}PHPh)$.[33]

(42) Strictly speaking, the ESR spectra of $I'^{-\cdot}$ and $II'^{-\cdot}$ are consistent with either the general structures A or B. The similarities of the ligand splittings

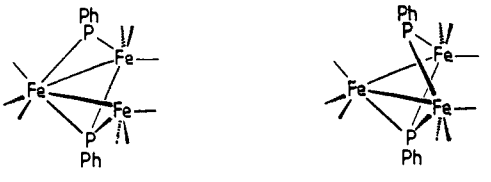

A B

$a_P(L)$ and the $\langle g \rangle$ values with those of the mononuclear $Fe(CO)_3L_2^+$ support the structure A containing a 17-electron iron center. For further discussion, see ref 35b.

(43) Baker, P. K.; Connelly, N. G.; Jones, B. M. R.; Maher, J. P.; Somers, K. R. *J. Chem. Soc., Dalton Trans.* **1980**, 579.

G) at $\langle g \rangle = 2.023$. The $\langle g \rangle$ value and triplet splitting in $II^{-\cdot}$ are akin to those observed for $I\cdot$ (see Table VI). Accordingly, the triplet splitting is assigned to the pair of equivalent μ_3-phosphidene caps in an analogous structure $II^{-\cdot}$. The structural relationship between $II^{-\cdot}$ and $II'^{-\cdot}$ in eq 14 is tantamount to the microscopic reverse of the ring opening of the parent anion radical in eq 11. As such, it is represented by the recapping of the triiron array by the conversion of the μ_2-bridge back to the μ_3-phosphinidene cap, i.e., eq 15.

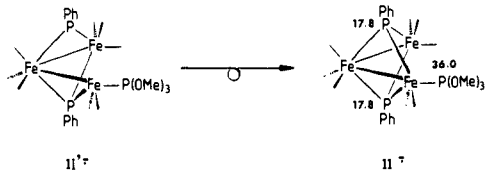

$II'^{-\cdot}$ $II^{-\cdot}$ (15)

In accord with this assignment, the anion radical $1I^{-\cdot}$ can also be generated directly by the reduction of the mono-phosphite II in tetrahydrofuran. For comparison, Table VI also includes the ESR spectral data of the isomeric anion radicals from the mono-triethylphosphine and triphenylphosphine derivatives.

Taken together, the foregoing ESR studies indicate that the anion radicals derived from the triiron clusters I, II, and V are of two types, which can be qualitatively described as the "closed" and "open" structures shown in eq 16 where L = CO, $P(OMe)_3$, PEt_3, etc. Such isomeric anion radicals are experimentally

closed open (16)

distinguished in their ESR spectra by the ^{31}P hyperfine splitting patterns and the magnitudes of the $\langle g \rangle$ values. Moreover the generality of these experimental probes for the structures of triiron clusters has been established by the inspection of a variety of other derivatives.[35] Since the closed structure is related to the open one simply by the scission of the bridging bond between a phosphinidene cap and an iron center, we believe that they are interconvertible—the position of the equilibrium being dependent on (a) the solvent polarity and (b) the salt concentration. For example, the parent cluster I and its mono-phosphite II upon reduction in acetonitrile initially afford the closed anion radicals $I^{-\cdot}$ and $II^{-\cdot}$, which spontaneously rearrange to the open anion radicals $I'^{-\cdot}$ and $II'^{-\cdot}$, respectively. By contrast, in tetrahydrofuran, the closed anion radicals $I^{-\cdot}$ and $II^{-\cdot}$ persist indefinitely when formed under equivalent conditions. However, this status is dramatically affected by the presence of salts such as tetra-*n*-butylammonium perchlorate (TBAP). Thus, the addition of 0.3 M TBAP to either $I^{-\cdot}$ or $II^{-\cdot}$ in THF is sufficient to lead to a steady-state population of anion radicals which consists primarily of the open structures $I'^{-\cdot}$ and $II'^{-\cdot}$, respectively (compare Figure 7). We infer from such observations that the open structure is stabilized relative to the closed structure of triiron anion radicals by polar environmental effects induced either by the solvent (e.g., acetonitrile) or a salt (e.g., TBAP in THF).[44]

D. Kinetics of the Catalytic Substitution. The rate and efficiency of the ETC substitution was examined in acetonitrile and THF solutions by electrochemically reducing at −0.80 V a small amount (10%) of $Fe_3(CO)_9(PPh)_2$ in the presence of excess trimethyl phosphite or triethylphosphine. The course of ligand substitution was monitored by following the disappearance of the reactant triiron cluster I by cyclic voltammetry, as described in the Experimental Section. Figure 8 shows the rates of ligand substitution under three typical conditions. The linear plots in all three cases illustrate the zero-order kinetics dependence on the concentration of $Fe_3(CO)_9(PPh)_2$. The pseudo-zero-order rate

(44) The negative charge is more localized in the open structure than in the closed structure. For the LUMO in closed trinuclear structures, see ref 10.

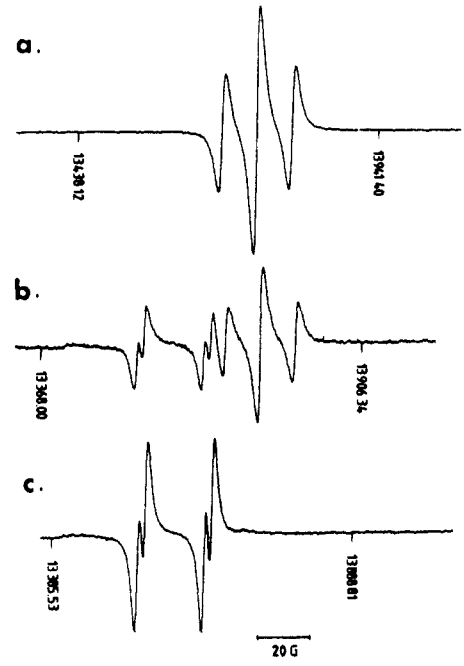

Figure 8. Salt effect on the interconversion $I^{-\cdot} \rightleftharpoons I'^{-\cdot}$. ESR spectra obtained from (a) reduction of I to $I^{-\cdot}$ with sodioamalgam in THF containing 0.3 M TBAP, (b) after 8 h, and (c) $I'^{-\cdot}$ after 24 h at 25 °C.

Table VII. Kinetics of ETC Ligand Substitution[a]

solvent	added ligand, M	k_{obsd}, M s^{-1}
THF	$P(OMe)_3$, 0.157	1.2×10^{-6}
THF	$P(OMe)_3$, 0.314	1.5×10^{-6}
THF	$P(OMe)_3$, 0.627	1.2×10^{-6}
THF	$P(OMe)_3$, 0.941	1.3×10^{-6}
THF	$P(OMe)_3$, 1.254	1.4×10^{-6}
CH_3CN	$P(OMe)_3$, 0.157	1.9×10^{-6}
CH_3CN	$P(OMe)_3$, 0.314	2.0×10^{-6}
CH_3CN	$P(OMe)_3$, 0.627	2.1×10^{-6}
CH_3CN	$P(OMe)_3$, 0.941	2.4×10^{-6}
CH_3CN	$P(OMe)_3$, 1.254	2.6×10^{-6}
THF	PEt_3, 0.126	1.3×10^{-6}
THF	PEt_3, 0.251	1.5×10^{-6}
THF	PEt_3, 0.377	1.9×10^{-6}
THF	PEt_3, 0.502	2.6×10^{-6}

[a] In a system consisting of 5.82×10^{-3} M $Fe_3(CO)_9(PPh)_2$ initiated by 5.82×10^{-4} M $Fe_3(CO)_9(PPh)_2^{-\cdot}$ generated by electrochemical reduction with 10% charge at 25 °C.

constants k_{obsd} are listed in Table VII for ETC ligand substitution carried out in either acetonitrile or THF with either trimethyl phosphite or triethylphosphine.

Discussion

The importance of electron-transfer catalysis (ETC) for the activation of polynuclear clusters lies in the efficiency and selectivity with which multiple processes such as ligand substitution can be carried out under mild conditions. Among the various systems extant, we believe that the bicapped triiron carbonyl $Fe_3(CO)_9(PPh)_2$ (I) offers an excellent opportunity to examine the pathways by which ETC effectively activates a metal cluster.

The stepwise ligand substitution of $Fe_3(CO)_9(PPh)_2$ to produce selectively the mono-, bis-, and tris-substitution products (II, III, and IV) according to eq 2, 3, and 4 is critically dependent on the potentials at which I, II, and III, respectively, are reduced in Table I. The electrochemical examination of $Fe_3(CO)_9(PPh)_2$ in Figure 2 demonstrates that the cluster undergoes two well-definied one-electron reductions as given by the 0/1− and 1−/2− redox couples in Table IV, i.e., eq 17. These well-behaved redox couples

$$\underset{I}{Fe_3(CO)_9(PPh)_2} \overset{+e}{\rightleftharpoons} \underset{I^{-\cdot}}{Fe_3(CO)_9(PPh)_2^{-\cdot}} \overset{+e}{\rightleftharpoons} \underset{I^{2-}}{Fe_3(CO)_9(PPh)_2^{2-}} \quad (17)$$

contrast with the behavior of the analogous binary iron carbonyl $Fe_3(CO)_{12}$ which barely undergoes reversible reduction.[45] The stabilizing effect in I may be attributed to the presence of a pair of bridging μ_3-phosphinidene caps which serve to maintain the cluster polyhedron intact. Indeed the widespread utilization of bridging ligands to preserve the integrity of polynuclear clusters derives from such observations. Otherwise, it is generally assumed that the bridging ligands play a largely innocent role in the determination of cluster reactivity.[46]

Our study of the triiron clusters indicates that the bridging ligand is intimately involved in electron-transfer catalysis of ligand substitution. Before proceeding with the mechanistic analysis of I, we note that the isoelectronic, sulfur-bridged cluster $Fe_3(CO)_9(\mu_3\text{-}S)_2$ undergoes a reversible one-electron reduction at a potential E^0 of −0.40 V which is significantly more positive than that required for I.[13,18] The second reduction of both clusters occurs at the same potential but is irreversible in the sulfur-bridged analogue. The difference between the two triiron cluster systems lies not only in the ability of the capping ligand to alter the redox potential E^0 but also to stabilize the reduced clusters. This distinction is also in evidence during electron-transfer catalysis of ligand substitution of the triiron clusters. For example, in the earlier study, Darchen and co-workers[13] found the electrocatalysis of ligand substitution of the sulfur-bridged triiron cluster $Fe_3(CO)_8(\mu_3\text{-}S)_2L$ to occur efficiently on the millisecond time scale, as shown by the alteration of the CV wave in the presence of added $P(OMe)_3$.[47] The detailed analysis of the heterogenous electrode kinetics associated with the cyclic voltammetry of such an electrocatalytic process[49,50] establishes the general mechanism of the chain process to consist of (a) the initiation step eq 18, followed

$$M_x(CO) \overset{E^0}{\rightleftharpoons} M_x(CO)^{-\cdot} \qquad (18)$$

by (b) the rapid catalytic cycle, Scheme I, which leads to (c) the overall ligand substitution in eq 21, where $M_x(CO)$ represents the

Scheme I

$$M_x(CO)^{-\cdot} + L \longrightarrow M_x(L)^{-\cdot} + CO \qquad (19)$$

$$M_x(L)^{-\cdot} + M_x(CO) \longrightarrow M_x(L) + M_x(CO)^{-\cdot}, \text{ etc.} \qquad (20)$$

metal carbonyl cluster undergoing substitution with the nucleophile L to afford the substituted cluster $M_x(L)$.

$$M_x(CO) + L \rightarrow M_x(L) + CO \qquad (21)$$

The ligand substitution of $Fe_3(CO)_9(PPh)_2$ (I) under ETC conditions parallels the electrocatalytic, stepwise replacement at the three separate iron centers in the sulfur-bridged cluster.[13] However, the rate of the chain process is slower in $Fe_3(CO)_9(PPh)_2$, as indicated by the insignificant perturbation of the cyclic voltammogram in Figure 4. Since the initiation step (eq 18) and the driving force for electron transfer (eq 20) pose no kinetic limitation,[51] the difference in the two systems must lie in the rates

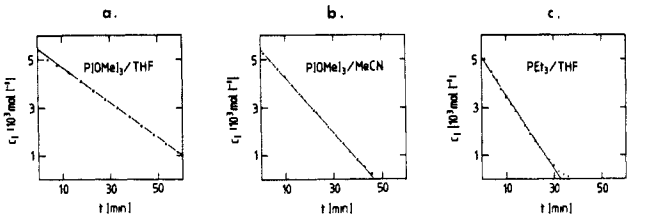

Figure 9. Pseudo-zero-order kinetics observed in the electrocatalytic ligand substitution of I in (a) THF containing 0.3 M TBAP and 0.16 M $P(OMe)_3$, (b) MeCN containing 0.1 M TBAP and 0.16 M $P(OMe)_3$, and (c) THF containing 0.3 M TBAP and 0.50 M PEt_3 after 10% reduction (t = 0) at 25 °C.

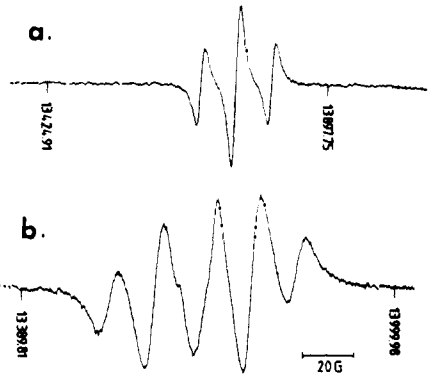

Figure 10. Identity of triiron anion radicals during ETC ligand substitution of I in THF with $P(OMe)_3$ at 25 °C. ESR spectra show the predominance of (a) $I^{-\cdot}$ at steady state and (b) $II^{-\cdot}$ at the final state (x10).

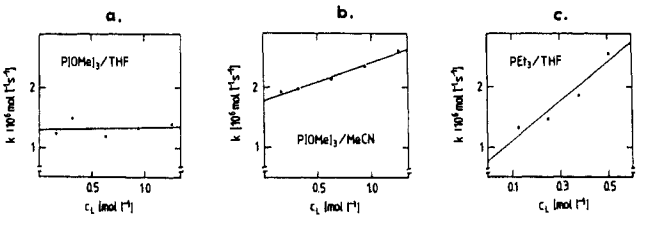

Figure 11. Ligand dependence of the rate constant k_{obsd} for ETC ligand substitution of $Fe_3(CO)_9(PPh)_2$ with (a) $P(OMe)_3$ in THF, (b) $P(OMe)_3$ in MeCN, and (c) PEt_3 in THF, under conditions given in Figure 9.

of the crucial step (eq 19) leading to substitution in the anion radical of the cluster itself. Indeed this fortuitous circumstance in $Fe_3(CO)_9(PPh)_2$ provides us now with a unique opportunity to examine the critical role of anion radicals in cluster substitution.

Among cluster anion radicals, the phosphinidene-capped $Fe_3(CO)_9(PPh)_2$ ($I^{-\cdot}$) is unusual in that its ESR spectrum shows a well-resolved nuclear hyperfine splitting arising from the capping ligands.[52] In particular, the magnitude and the hyperfine splitting patterns for the ^{31}P nucleus, together with the isotropic $\langle g \rangle$ values, provide invaluable structural probes with which to establish the four distinctive anion radicals in eq 10, 11, 12, and 15. Transient ESR studies show that the ligand substitution attendant upon the exposure of the anion radical $I^{-\cdot}$ to $P(OMe)_3$ in eq 13 proceeds in two discrete steps. Thus, the formulation in eq 14 consists of a prior opening of the cluster $I^{-\cdot}$ to expose a coordinatively unsaturated 17-electron iron center, which is followed by the rapid association with the nucleophile to afford the substitution product in an open configuration. Coupled to the subsequent reestablishment of the closed cluster (eq 15), the stepwise sequence is

(45) Bond, A. M.; Dawson, P. A.; Peake, B. M.; Robinson, B. H.; Simpson, J. *Inorg. Chem.* **1977**, *16*, 2199.

(46) See, e.g.: (a) Huttner, G.; Schneider, J.; Müller, H.-D.; Mohr, G.; von Seyerl, J.; Wohlfarth, L. *Angew. Chem.* **1979**, *91*, 82. (b) Schneider, J.; Huttner, G. *Chem. Ber.* **1983**, *116*, 917.

(47) See also the ETC studies by Rieger, Robinson, Simpson, and coworkers on cobalt clusters in ref 12a and 48.

(48) (a) Arewgoda, M.; Rieger, P. H.; Robinson, B. H.; Simpson, J.; Visco, S. J. *J. Am. Chem. Soc.* **1982**, *104*, 5633. (b) Arewgoda, M.; Robinson, B. H.; Simpson, J. *J. Chem. Soc., Chem. Commun.* **1982**, *284*. (c) Cunninghame, R. G.; Downard, A. J.; Hanton, L. R.; Jensen, S. D.; Robinson, B. H.; Simpson, J. *Organometallics* **1984**, *3*, 180. (d) Reference 14. (e) See also: Bruce, M. I.; Matisons, J. G.; Nicholson, D. K. *J. Organomet. Chem.* **1983**, *247*, 321.

(49) (a) Garreau, D.; Saveánt, J. M. *J. Electroanal. Chem.* **1972**, *35*, 309. (b) Garreau, D.; Saveánt, J. M. *J. Electroanal. Chem.* **1974**, *50*, 1. (c) Saveánt, J. M.; Thiebault, A. *J. Electroanal. Chem.* **1979**, *103*, 303.

(50) (a) Hershberger, J. W.; Klingler, R. J.; Kochi, J. K. *J. Am. Chem. Soc.* **1983**, *105*, 61. (b) Zizelman, P. M.; Amatore, C.; Kochi, J. K. *J. Am. Chem. Soc.* **1984**, *106*, 3771.

(51) The exergonic driving force is indicated by the relative values of E^0 for I and II in Table IV. For the relationship between ΔG and the rate of electron transfer, see related papers to: Klingler, R. J.; Kochi, J. K. *J. Am. Chem. Soc.* **1981**, *103*, 5839. For the effect of phosphine ligands on the redox potentials of metal carbonyls, see: Hershberger, J. W.; Kochi, J. K. *Polyhedron* **1983**, *2*, 929.

(52) Compare the ESR studies in ref 7 and 8.

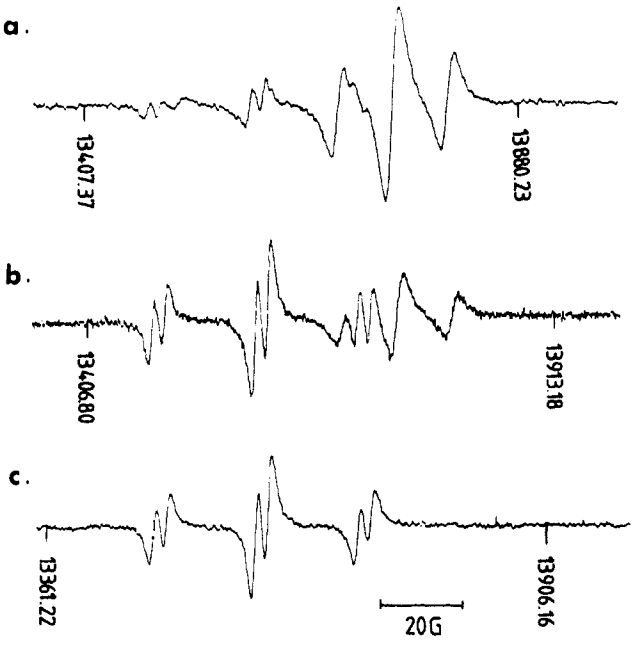

Figure 12. Identity of triiron anion radicals during ETC ligand substitution of I with $P(OMe)_3$ in acetonitrile at 25 °C. ESR spectrum in (a) shows the steady-state population of $I^{-\cdot}$ and $II'^{-\cdot}$ during the catalytic cycle. The emergence of $II'^{-\cdot}$ as the dominant species toward the end and at the end of the ligand substitution is shown by the ESR spectra (b) and (c), respectively.

Scheme II

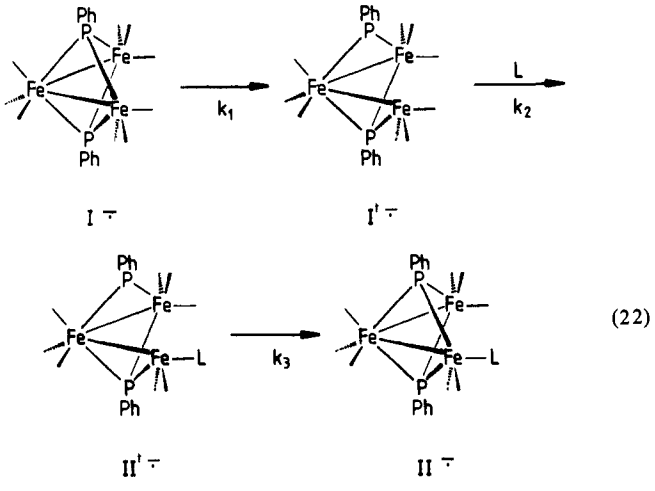

(22)

depicted as in Scheme II. The clean delineation of the individual steps in Scheme II by transient ESR spectroscopy coincides with the overall transformation in eq 23, which is tantamount to the rate-limiting process in eq 19, Scheme I.

$$Fe_3(CO)_9(\mu_3\text{-}PPh)_2^{-\cdot} + P(OMe)_3 \xrightarrow{k} Fe_3(CO)_8(\mu_3\text{-}PPh)_2[P(OMe)_3]^{-\cdot} + CO \quad (23)$$

($I^{-\cdot}$ → $II^{-\cdot}$)

The incorporation of such a ligand substitution of anion radicals in the ETC mechanism is depicted in Scheme III. According to Scheme III, the steady-state population of the various triiron anion radicals is determined by the magnitudes of the rate constants in eq 22 together with the rate constant for electron transfer in eq 24. The ESR spectrum obtained at steady state during ETC

$$Fe_3(CO)_9(PPh)_2 + II^{-\cdot} \xrightarrow{k_4} II + Fe_3(CO)_9(PPh)_2^{-\cdot} \quad (24)$$

ligand substitution of $Fe_3(CO)_9(PPh)_2$ with $P(OMe)_3$ in tetrahydrofuran is shown in Figure 9a. The predominant anion radical under these conditions is clearly the closed $I^{-\cdot}$. This observation is consistent with the opening of the cluster, that is, rearrangement (eq 11) being the rate-limiting process (or stated in terms of the rate constant, $k_1 \ll k_2[L], k_3, k_4[I]$). This conclusion is strongly supported by the zero-order kinetic dependence of the experimental rate constant k_{obsd} on phosphite concentration, as shown in Figure 11a.[53]

The steady-state ESR spectrum measured in acetonitrile under the same conditions is shown in Figure 12a. It shows that the closed reactant $I^{-\cdot}$ is also the predominant form of the anion radical, but the presence of ~10% of the open product $II'^{-\cdot}$ is unmistakable. Coupled with observation of a phosphite-dependent component of the experimental rate constant (Figure 11b),[53] we tentatively suggest the competition from a bimolecular pathway for substitution in eq 13 which involves a direct attack on $I^{-\cdot}$ by $P(OMe)_3$,[54] i.e., eq 25. The trend shown in Figure 11c indicates

$$Fe_3(CO)_9(\mu_3\text{-}PPh)_2^{-\cdot} + P(OMe)_3 \xrightarrow{k_{1'}} Fe_3(CO)_8(\mu_3\text{-}PPh)(\mu_2\text{-}PPh)[P(OMe)_3] + CO \quad (25)$$

($I^{-\cdot}$ → $II'^{-\cdot}$)

that this bimolecular component is even more important with triethylphosphine in measure with it being a more powerful nucleophile than trimethyl phosphite.[55] As expected from the solvent effect on anion radical stability, the ESR spectrum recorded at the end of the catalytic cycle consists solely of that arising from $II^{-\cdot}$ in tetrahydrofuran (Figure 10b) and from $II'^{-\cdot}$ in acetonitrile (Figure 12c). The observation of the product anion radicals only at the end of the reaction is consistent with the rate of electron transfer being fast in this system. Such facile rates of electron transfer are consistent with the exergonic driving force $-\Delta G = \mathcal{F}\Delta E^0$ evaluated from the relative redox potentials ΔE^0 for the reactant and product in Table IV.

Summary and Conclusion

Electron-transfer catalysis of ligand substitution as examined in the triiron cluster $Fe_3(CO)_9(PPh)_2$ (I) affords selectively the mono-, bis-, and tris-substitution products with trimethyl phosphite in good yields. X-ray crystallography and ^{31}P NMR spectroscopy establish the stepwise substitution of the CO ligands to occur selectively at three separate iron centers. Electrocatalysis of ligand substitution parallels the route previously established in the sulfur-bridged analogue $Fe_3(CO)_8(\mu_3\text{-}S)_2L$.[13] As such, the ETC mechanism[56] depicted in eq 18 and Scheme I also applies to $Fe_3(CO)_9(PPh)_2$. In accord with this catalytic mechanism, we find the selectivity in ligand substitution to be determined by the redox potential established in eq 18 for the initiation step. The observation of four discrete anion radicals by kinetic ESR spectroscopy establishes the sequence of paramagnetic intermediates in Scheme II for the ligand substitution process (eq 19). Analysis of the steady-state ESR spectra together with the measurement of the kinetics of the catalytic system strongly points to the slippage of a μ_3-phosphinidene bridge to a μ_2-ligand as in eq 11 to be the rate-limiting factor in cluster substitution. This conclusion con-

(53) Figure 10, the intercepts are (a) 1.30 ± 0.26, (b) 1.78 ± 0.08, and (c) 0.76 ± 1.60 × 10^{-6} M s^{-1} and the slopes are 0.04 ± 0.34, 0.63 ± 0.10, and 3.3 ± 0.55 × 10^{-6} s^{-1}, respectively.

(54) (a) For a similar process in a tetracobalt cluster $Co_4(CO)_{10}(PPh)_2^{-\cdot}$, see: Richmond, M. R.; Kochi, J. K. *Inorg. Chem.* **1986**, *25*, 656. (b) Alternatively, it is possible in Scheme III that the electron-transfer step is (in part) between $II'^{-\cdot}$ and I. Although not rigorously ruled out by the data on hand, we disfavor this possibility, since cyclic voltammetry shows that the oxidation of the open anion radical $I'^{-\cdot}$ is irreversible, the peak potential (E_p) of the anodic wave at ~−0.3 V being about 500 mV more positive than that of the closed anion radical $I^{-\cdot}$. We expect the same relationship to hold for the phosphine derivatives $II'^{-\cdot}$ and $II^{-\cdot}$. Such a large positive shift in the anodic potential upon rearrangement is not unreasonable if one considers that $I^{-\cdot}$ and $II^{-\cdot}$ are "electron excess" clusters whereas the open analogues $I'^{-\cdot}$ and $II'^{-\cdot}$ contain electron-deficient 17-electron centers. Thus, the rearrangement $II'^{-\cdot}$ → $II^{-\cdot}$ is required to facilitate electron transfer to I.

(55) As judged by their pK_a values. See footnote 36 in ref 50b.

(56) For general discussion of ETC mechanisms, see: (a) Chanon, M.; Tobe, M. L. *Angew. Chem., Int. Ed. Engl.* **1982**, *21*, 1. (b) Bunnett, J. F. *Acc. Chem. Res.* **1978**, *11*, 413. (c) Saveant, J. M. *Acc. Chem. Res.* **1980**, *13*, 323. (d) Chanon, M. *Bull. Soc. Chim. Fr.* **1982**, 197.

Scheme III

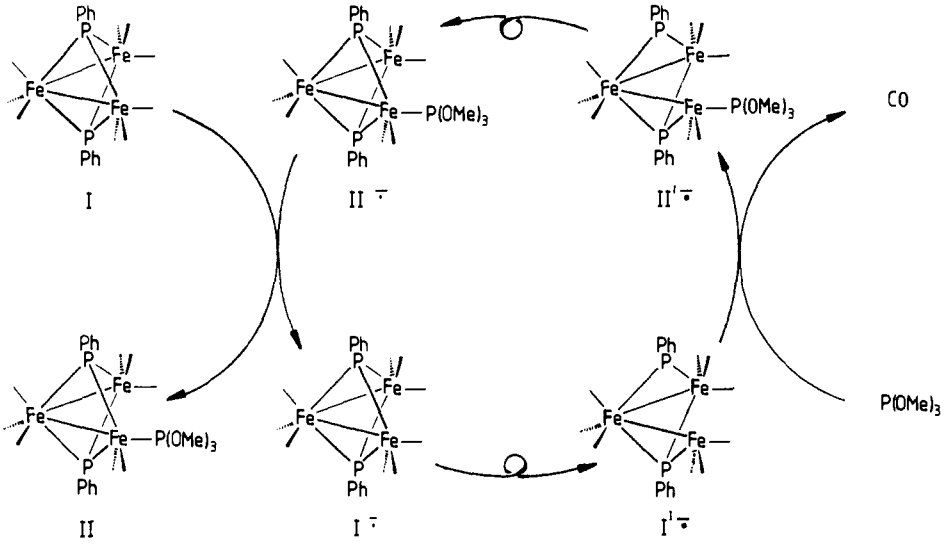

trasts with the fragmentation of metal–metal bonds or dissociative CO loss in other cluster systems undergoing ETC substitution. However, they all share in common the formation of 17-electron coordinatively unsaturated metal centers as an important facet of cluster reactivity. In this regard, electron-transfer catalysis of ligand substitution in polynuclear clusters is to be distinguished from the slower, dissociative and associative pathways extant in the more traditional thermal processes.[57] These ETC studies emphasize the critical, active role played by the capping ligand in cluster reactivity. We hope that this mechanistic insight as such will encourage the deliberate design of capping ligands to optimize this function rather than to consider them merely in a passive role.[4,58]

Experimental Section

Materials. Iron pentacarbonyl and phenyldichlorophosphine (Strem Chemical) were used as received. Trimethyl phosphite (Victor Chemical) and triethylphosphine (M and T Chemical) were distilled from sodium and stored under an argon atmosphere. The triiron cluster $Fe_3(CO)_9(PPh)_2$ was prepared by the procedure described by Treichel et al.:[19] mp 132–134 °C. $^{31}P\{^1H\}$ NMR ($CDCl_3$): δ 317 (s) IR (hexane) ν(CO): 2044 (s), 2023 (s), 2008 (s), 1996 (m), and 1986 (w) cm^{-1}. Tetra-*n*-butylammonium perchlorate (G. F. Smith Chemical) was recrystallized from a mixture of hexane and ethyl acetate and dried in vacuo prior to use. Silica gel (60–200 mesh) from J. T. Baker was used for column chromatography.

All manipulations were carried out under argon with the aid of standard Schlenk line techniques. Solvents were purified by standard procedures.[59] Melting points are not corrected. Elemental analyses were performed by Atlantic Microlab, Inc., Atlanta, GA.

Instrumentation. The ^1H (89.55 MHz) and ^{31}P (36.23 MHz) NMR spectra were recorded on a JEOL FX-90Q spectrometer. Infrared spectra were obtained on a Nicolet DX-10 FT spectrometer. The X-band ESR spectra were recorded on a Varian Century-line E112 spectrometer equipped with a NMR gaussmeter for field frequency calibration. Cyclic voltammetry was performed at a platinum electrode with an IR-compensated potentiostat[49] driven by a Princeton Applied Research Model 175 universal programmer. Cyclic voltammograms were recorded on a Houston Series 2000 *X-Y* recorder. The $E_{1/2}$ and E_p values were determined by cyclic voltammetry and referred to SCE. The reference electrode was in contact with the solution by a cracked glass tip. The bulk electrolysis cell was of air-tight design with high vacuum Teflon valves (Kontes) and viton o-ring seals to allow an inert atmosphere to be maintained without contamination by grease.

Crystallographic Analysis of the Triiron Tris-Phosphite IV. A large carmine-red triangular plate of dimensions 0.50 × 0.50 × 0.15 mm (obtained by the slow solvent evaporation of a mixture of hexane and methylene chloride) was mounted on a glass fiber in a random orientation on an Enraf-Nonius CAD-4 automatic diffractometer. The radiation used was Mo Kα monochromatized by a dense graphite crystal assumed for all purposes to be 50% imperfect. The *Laue* symmetry was determined to be 1, and the space group was shown to be either $P1$ or $P\bar{1}$. To reduce the data, Lorentz and polarization factors were applied; however, no correction for absorption was made. The collection and processing parameters are as follows: space group, $P\bar{1}$, triclinic; cell constants a = 10.539 (1) Å, b = 10.749 (2) Å, c = 18.726 (4) Å; α = 85.14 (2)°, β = 75.50 (1)°, γ = 68.53 (1)°; V = 1911 Å^3; molecular formula, $Fe_3P_5O_{15}C_{27}H_{37}$; formula weight, 924.0; formula units per cell, Z = 2; density (ρ), 1.61 g cm^{-1}; absorption coefficient (μ), 13.91 cm^{-1}; radiation (Mo Kα) (λ), 0.710 73 Å; total data collected, 2403; independent data ($I > 3\sigma(I)$), 2091; total variables, 451; $R = \sum||F_o| - |F_c||/\sum|F_o|$, 0.038; $R_w = [\sum w(|F_o| - |F_c|)^2/\sum_w|F_o|^2]^{1/2}$, 0.045; weights $w = \sigma(F) - 2$.

The structure was solved by SIMPEL-82[60] which revealed the positions of all three iron and five phosphorus atoms in the asymmetric unit. All other non-hydrogen atoms were located in subsequent difference Fourier synthesis. The usual sequence of isotropic and anisotropic refinement was followed, after which all hydrogens were entered in ideally calculated positions. All calculations were made by using Molecular Structure Corporation's TEXRAY 230 modifications of the SDP-PLUS series of programs. The fractional atomic coordinates and anisotropic thermal parameters are included in Table VIII.

Synthesis of $Fe_3(CO)_8(\mu\text{-PPh})_2(P(OMe)_3)$ (II). To an argon-flushed electrolysis cell was added 200 mg (0.314 mmol) of $Fe_3(CO)_9(\mu\text{-PPh})_2$, followed by 25 mL of THF containing 0.3 M TBAP and 2 mL (17.0 mmol) of $P(OMe)_3$. The electrocatalytic reaction was initiated by passage of ~2.0 mA of cathodic current in the constant-current mode through the stirred solution. The initial potential of -0.78 V shifted to -0.84 V during the passage of 5% of the theoretical charge required for the amount of $Fe_3(CO)_9(\mu\text{-PPh})_2$ used. The extent of the substitution reaction was monitored by cyclic voltammetry. After an hour at room temperature, the substitution reaction was complete. The solution was reoxidized by passage of ~ 2.0 mA of anodic current in the constant-current mode until the potential had shifted to -0.2 V. The solution was evaporated to dryness and the residue extracted with a 1:1 mixture of hexane and benzene and filtered through 3 cm of silica gel. The filtrate was concentrated and chromatographed on silica gel (3 × 10 cm). The product was eluted with a 3:1 mixture of hexane and benzene. Crystallization from hexane gave 150 mg (65%) of II as red needles: mp 141 °C. ^1H NMR ($CDCl_3$): δ 7.70–7.30 (m, C_6H_5), 3.62 (d, $^3J_{PH}$ = 12.0 Hz, OCH_3), 3.48 (d, $^3J_{PH}$ = 12.0 Hz, OCH_3). IR (toluene) ν(CO): 2056 (m), 2016 (s), 1996 (s), 1966 (br) cm^{-1}. Anal. Calcd for $C_{23}H_{19}Fe_3$-

(57) See: (a) Cetini, G.; Stanghellini, P. L.; Rossetti, R.; Gambino, O. *J. Organomet. Chem.* **1968**, *15*, 373. (b) Cetini, G.; Stanghellini, P. L.; Rossetti, R.; Gambino, O. *Inorg. Chim. Acta* **1968**, *2*, 433. (c) Rossetti, R.; Stanghellini, P. L.; Gambino, O.; Cetini, G. *Inorg. Chim. Acta* **1972**, *6*, 205. (d) Rossetti, R.; Gervasio, G.; Stanghellini, P. L. *J. Chem. Soc., Dalton Trans.* **1978**, 222. (e) Lesch, D. A.; Rauchfuss, T. B. *Organometallics* **1982**, *1*, 499. And ref 10–15 cited therein.

(58) For example see: Knoll, K.; Huttner, G.; Zsolnai, L.; Jibril, I.; Wasiucionek, M. *J. Organomet. Chem.* **1985**, *294*, 91. And Schneider, J.; Minelli, M.; Huttner, G. *J. Organomet. Chem.* **1985**, *294*, 75.

(59) Perrin, D. D.; Armarego, W. L.; Perrin, D. R. *Purification of Laboratory Chemicals*; Pergamon: New York, 1980.

(60) Kiers, C., Department of Crystallography, University of Amsterdam, 1982.

Table VIII. Fractional Atomic Coordinates and Isotropic Thermal Parameters for Non-Hydrogen Atoms of the Tris-Phosphite IV[a]

atom	x	y	z	B, Å²	atom	x	y	z	B, Å²
Fe1	0.9790 (1)	0.2941 (1)	0.65540 (7)	2.35 (3)	C22	1.2084 (8)	−0.0464 (7)	0.6674 (4)	2.3 (2)
Fe2	1.0990 (1)	0.2523 (1)	0.76999 (7)	2.11 (3)	C23	1.1942 (9)	−0.1702 (8)	0.6752 (5)	3.6 (3)
Fe3	0.9315 (1)	0.1056 (1)	0.82335 (7)	2.21 (3)	C24	1.304 (1)	−0.2831 (9)	0.6461 (6)	4.7 (3)
P1	0.8699 (2)	0.3102 (2)	0.7749 (1)	2.09 (6)	C25	1.428 (1)	−0.2749 (9)	0.6084 (6)	5.6 (3)
P2	1.0628 (2)	0.0997 (2)	0.7102 (1)	2.21 (6)	C26	1.4472 (9)	−0.154 (1)	0.5992 (6)	5.1 (3)
P3	0.8227 (2)	0.2645 (2)	0.6124 (1)	3.09 (7)	C27	1.8848 (9)	−0.0401 (8)	0.6289 (5)	4.0 (3)
P4	1.0712 (2)	0.3784 (2)	0.8601 (1)	2.75 (7)	H7A	0.7497	0.4930	0.4723	5*
P5	0.7812 (2)	0.0216 (2)	0.8131 (1)	2.87 (7)	H7B	0.8851	0.4559	0.5082	5*
O1	0.8968 (7)	0.5834 (6)	0.6315 (4)	5.7 (2)	H7C	0.8693	0.3431	0.4615	5*
O2	1.1967 (6)	0.2244 (6)	0.5198 (3)	5.1 (2)	H8A	0.8689	0.0074	0.4964	5*
O3	1.3460 (6)	0.0424 (6)	0.8021 (4)	5.3 (2)	H8B	0.7262	0.0761	0.5600	5*
O4	1.2473 (6)	0.3960 (6)	0.6643 (3)	4.8 (2)	H8C	0.7692	0.1627	0.4884	5*
O5	1.1362 (6)	−0.1433 (6)	0.8619 (4)	5.2 (2)	H9A	0.4925	0.2727	0.7112	5*
O6	0.7917 (7)	0.1795 (6)	0.9760 (3)	5.1 (2)	H9B	0.5143	0.3906	0.6540	5*
O7	0.7410 (6)	0.3789 (6)	0.5630 (3)	4.8 (2)	H9C	0.5481	0.2419	0.6227	5*
O8	0.8840 (6)	0.1351 (6)	0.5625 (3)	5.7 (2)	H10A	1.3235	0.4746	0.9050	5*
O9	0.6917 (6)	0.2541 (6)	0.6704 (3)	5.1 (2)	H10B	1.1626	0.5728	0.9059	5*
O10	1.2176 (5)	0.3912 (5)	0.8601 (3)	3.7 (2)	H10C	1.1923	0.4495	0.9641	5*
O11	1.0130 (6)	0.3419 (5)	0.9431 (3)	3.8 (2)	H11A	1.0417	0.2149	1.0271	5*
O12	0.9639 (5)	0.5299 (5)	0.8693 (3)	3.6 (2)	H11B	1.1067	0.1430	0.9460	5*
O13	0.7569 (6)	−0.0688 (5)	0.8839 (3)	4.1 (2)	H11C	1.1865	0.2263	0.9750	5*
O14	0.6258 (5)	0.1101 (5)	0.8079 (3)	3.7 (2)	H12A	0.9009	0.7077	0.8207	5*
O15	0.8244 (6)	−0.0720 (6)	0.7438 (3)	4.5 (2)	H12B	1.0689	0.6231	0.7942	5*
C1	0.9263 (9)	0.4729 (9)	0.6418 (5)	3.8 (3)	H12C	0.9573	0.5804	0.7646	5*
C2	1.1098 (9)	0.2516 (8)	0.5748 (5)	3.1 (3)	H13A	0.6548	−0.1771	0.9476	5*
C3	1.2484 (8)	0.1256 (8)	0.7899 (5)	3.3 (3)	H13B	0.5557	−0.0512	0.9076	5*
C4	1.1830 (8)	0.3403 (8)	0.7044 (5)	3.0 (3)	H13C	0.6627	−0.1850	0.8598	5*
C5	1.0542 (8)	−0.0458 (8)	0.8477 (5)	2.7 (2)	H14A	0.4470	0.2575	0.8496	5*
C6	0.8480 (8)	0.1523 (8)	0.9143 (4)	2.6 (2)	H14B	0.5288	0.1712	0.9112	5*
C7	0.818 (1)	0.421 (1)	0.4960 (6)	6.9 (4)	H14C	0.5872	0.2785	0.8599	5*
C8	0.806 (1)	0.092 (1)	0.5240 (6)	7.7 (4)	H15A	0.7963	−0.1630	0.6658	5*
C9	0.551 (1)	0.293 (1)	0.6640 (6)	6.4 (4)	H15B	0.6776	−0.1428	0.7434	5*
C10	1.225 (1)	0.4791 (9)	0.9131 (6)	5.7 (3)	H15C	0.6767	−0.0156	0.6890	5*
C11	1.093 (1)	0.223 (1)	0.9753 (5)	5.6 (3)	H17	0.6574	0.5218	0.7180	5*
C12	0.974 (1)	0.6170 (9)	0.8074 (6)	6.5 (4)	H18	0.4551	0.6995	0.7715	5*
C13	0.649 (1)	-0.125 (1)	0.9010 (6)	6.4 (3)	H19	0.3935	0.7429	0.8966	5*
C14	0.5409 (9)	0.2121 (9)	0.8613 (7)	6.1 (4)	H20	0.5338	0.6058	0.9717	5*
C15	0.737 (1)	−0.100 (1)	0.7079 (6)	7.3 (4)	H21	0.7348	0.4297	0.9212	5*
C16	0.7177 (8)	0.4560 (7)	0.8147 (4)	2.1 (2)	H23	1.1074	−0.1776	0.7011	5*
C17	0.6332 (8)	0.5381 (8)	0.7698 (5)	2.8 (3)	H24	1.2934	−0.3676	0.6522	5*
C18	0.5129 (8)	0.6440 (8)	0.8022 (5)	3.6 (3)	H25	1.5040	−0.3537	0.5877	5*
C19	0.4759 (9)	0.6699 (8)	0.8761 (5)	3.4 (3)	H26	1.5346	−0.1473	0.5731	5*
C20	0.5591 (8)	0.5890 (7)	0.9202 (5)	2.9 (3)	H27	1.3461	0.0442	0.6226	5*
C21	0.6782 (8)	0.4842 (7)	0.8898 (5)	2.6 (2)					

[a] Anisotropically refined atoms are given in the form of the isotropic equivalent thermal parameter defined as $^4/_3[a^2B(1,1) + b^2B(2,2) + c^2B(3,3) + ab(\cos\gamma)B(1,2) + ac(\cos\beta)B(1,3) + bc(\cos\alpha)B(2,3)]$. Asterisk identifies atom refined isotropically.

$O_{11}P_3$ (731.9): C, 37.75; H, 2.62. Found: C, 37.51; H, 2.65.

Synthesis of $Fe_3(CO)_7(\mu\text{-PPh})_2[P(OCH_3)_3]_2$ (III). The synthesis with 200 mg (0.314 mmol) of **I** followed a similar procedure to that described above in acetonitrile containing 0.1 M TBAP or in THF containing 0.3 M TBAP. Electrochemical conditions are given in Table I. Each ligand substitution step was monitored by cyclic voltammetry. The product was purified by chromatography on silica gel (3 × 10 cm, hexane/benzene 1:1). Crystallization from a 4:1 mixture of hexane and toluene yielded 164 mg (63%) of red microcrystalline $Fe_3(CO)_7(PPh)_2[P(OCH_3)]_2$. ^1H NMR ($CDCl_3$): δ 7.80-7.35 (m, C_6H_5), 3.59 (d, $^3J_{PH}$ = 11.4 Hz, OCH_3), and 3.41 (d, $^3J_{PH}$ = 11.5 Hz, OCH_3). IR (toluene) ν(CO): 2028 (m), 1990 (s), 1981 (s), 1961 (s), 1949 (sh), and 1932 (m) cm^{-1}. Anal. Calcd for $C_{25}H_{28}Fe_3O_{13}P_4$ (827.9): C, 36.27; H, 3.41. Found: C, 36.07; H, 3.47.

The temperature-dependent ^{31}P NMR spectrum of the bis-phosphite III clearly shows the presence of two isomers (Table III). Neither the infrared nor the ^{31}P NMR spectra accord with the data reported for the 1,1-bis(phosphite) by Muetterties et al.[20] At room temperature, only isomer IIIa shows a well-resolved ^{31}P NMR spectrum in $CDCl_3$. The presence of additional broad signals indicate the coalescence of IIIb and IIIc. However, at −66 °C, the conformational isomers resulting from the axial and equatorial phosphites on the basal iron centers are frozen out in their (solution) equilibrium population. The isomeric composition of the mixture of IIIa:IIIb:IIIc is 75:5:20 by integration of the NMR resonances.

Synthesis of $Fe_3(CO)_6(\mu\text{-PPh})_2[P(OCH_3)_3]_3$ (IV). The synthesis followed a similar procedure to that described above in acetonitrile containing 0.1 M TBAP starting with 333 mg (0.402 mmol) of $Fe_3(CO)_7(PPh)_2[P(OCH_3)_3]_2$. While the solution was electrolyzed with a cathodic current of 12.93 mA in the constant-current mode for 50 min, the initial potential of -1.5 V rose to −1.8 V as the substitution reaction proceeded. The product was purified by chromatography on silica gel (3 × 10 cm, hexane and benzene (2:1)). Crystallization from a 4:1 mixture of hexane and CH_2Cl_2 gave 146 mg (39%) of dark-red crystals of IV: mp 240 °C. ^1H NMR ($CDCl_3$): δ 7.9–7.2 (m, C_6H_5), 3.54 (d, $^3J_{PH}$ = 12.2 Hz, $P(OCH_3)_3$), and 3.40 (d, $^3J_{PH}$ = 12.2 Hz, $P(OCH_3)_3$). IR (toluene) ν(CO): 2003 (m), 1977 (s), 1958 (m), and 1935 (m) cm^{-1}. Anal. Calcd for $C_{27}H_{37}Fe_3O_{15}P_5$ (924.0): C, 35.10; H, 4.04. Found: C, 34.88; H, 4.06.

Synthesis of $Fe_3(CO)_8(\mu\text{-PPh})_2[P(C_2H_5)_3]$ (V). The synthesis followed a similar procedure to that described above in THF containing 0.3 M TBAP starting with 200 mg (0.314 mmol) of I. Electrochemical conditions are given in Table I. The product was purified by chromatography on silica gel (3 × 10 cm, hexane and benzene (4:1)). Crystallization from hexane yielded 151 mg (66%) of dark-red crystals: mp 173 °C. ^1H NMR ($CDCl_3$): δ 7.8-7.3 (m, PC_6H_5), 1.88 (dq, $^2J_{PH}$ = 7.8, J_{HH} = 7.8 Hz, CH_2), 0.75 (dt, $^3J_{PH}$ = 16.1, $^3J_{HH}$ = 7.8 Hz, CH_3). IR (hexane) ν(CO): 2054 (m), 2013 (s), 1997 (s), 1992 (s), 1956 (m), and 1950 (m) cm^{-1}. Anal. Calcd for $C_{26}H_{25}Fe_3O_8P_3$(725.9): C, 43.02; H, 3.47. Found: C, 43.08; H, 3.51.

Synthesis of $Fe_3(CO)_7(\mu\text{-PPh})_2[P(C_2H_5)_3]_2$ (VI). The synthesis followed a similar procedure to that as described above in CH_3CN containing 0.1 M TBAP starting with 200 mg (0.314 mmol) of **I**. Electrochemical conditions are given in Table I. Each ligand substitution step was monitored by CV. The product was purified by chromatography on silica gel (3 × 10 cm, hexane/benzene (1:1)). Crystallization from hexane yielded 165 mg (58%) of dark-red crystals of $Fe_3(CO)_7(PPh)_2[P(C_2H_5)_3]_2$. ^1H NMR (CDL_3): δ 7.8-7.3 (m, $P(C_6H_5)$), 2.0–1.3 (m, CH_2), 1.2–0.5 (m, CH_3). IR (hexane) ν(CO): 2021 (m), 1983 (s), 1968 (s), 1954 (m), 1942 (m), and 1912 (m) cm^{-1}. Anal. Calcd for C_{31}-

$H_{40}Fe_3O_7P_4$ (816.1): C, 45.62; H, 4.94. Found: C, 45.52; H, 4.99.

The ^{31}P NMR spectrum of the bis-phosphine VI at -64 °C is consistent with the presence of two isomers VIa and VIc (analogous to IIIa and IIIc for the phosphite analogues, vide supra) in a 30:70 ratio. Although the line shape of VIa is unaffected by temperature variations, the signals of VIc are broadened at room temperature, and coalescence is observed at 53 °C in C_6D_6. There was no evidence for isomer VIb (corresponding to IIIb) at -64 °C. This coupled with the higher temperatures required for the interconversion of VIc with VIb suggests that the (axial, axial) conformation of basal phosphines in conformation VIb is disfavored relative to the (axial, equatorial) conformation in VIc. Nonbonded steric interactions, which are expected to be more severe with triethylphosphine relative to trimethyl phosphite,[61] are presumably responsible for the difference between IIIa and VIa, since the axial position is favored in the mono-substituted triiron clusters.[20,28]

Preparation of ESR Samples. Solutions of the anion radicals were prepared at room temperature under an argon atmosphere. They were transferred with the aid of a hypodermic syringe into ESR tubes, which were subsequently sealed under vacuum. For the description of the ESR technique, see ref 62.

Kinetic Measurements. In a bulk electrolysis cell, the solvent, electrolyte, and ligand were placed to obtain a total volume of 27 mL. This solution was prereduced at a potential of -2.0 V. Then 100 mg (0.157 mmol) of $Fe_3(CO)_9(PPh)_2$ was added. The CV of this solution was taken, and the peak current of the first reduction wave of $Fe_3(CO)_9(PPh)_2$ was used as a reference for the initial concentration of the parent cluster. In the constant current mode (2.529 mA), the solution was reduced for 10 min at a potential of -0.8 V corresponding to a reduction of 10% of $Fe_3(CO)_9(PPh)_2$. After electrolysis, the substitution reaction was followed by cyclic voltammetry taken at intervals varying between 2 and 5 min, until the starting material was consumed. The actual concentrations of unreacted starting material were calculated by direct comparison of the peak current of the first reduction wave of $Fe_3(CO)_9(PPh)_2$. Ligand substitutions of the parent cluster were mostly completed within 30-70 min after electrolysis. The solvent and electrolyte consisted of either tetrahydrofuran containing 0.3 M TBAP or acetonitrile containing 0.1 M TBAP. Varying amounts of ligand were added in measured amounts with the aid of a hypodermic syringe.

(61) Cone angle of PEt_3 = 132°, $P(OMe)_3$ = 107°. See: Tolman, C. A. *Chem. Rev.* **1977**, *77*, 313.
(62) Lau, W.; Huffman, J. C.; Kochi, J. K. *Organometallics* **1982**, *1*, 155.

Acknowledgment. We thank J. D. Korp for the crystal structure of IV, M. R. Richmond for helpful discussions, and the National Science Foundation and Robert A. Welch Foundation for financial support. H. H. Ohst is a recipient of a NATO grant administered under the auspices of the German Academic Exchange Service.

Registry No. I, 38903-71-8; $I^{-\cdot}$, 101198-33-8; $I'^{-\cdot}$, 101011-28-3; $II^{-\cdot}$, 39040-36-3; $II'^{-\cdot}$, 101011-23-8; IIa, 101011-13-6; IIb, 101011-14-7; IIIa, 101011-15-8; IIIb, 101011-16-9; IIIc, 101141-53-1; IVa, 101011-17-0; IVb, 101141-54-2; $V^{-\cdot}$, 101011-27-2; $V'^{-\cdot}$, 101011-25-0; Va, 101011-18-1; Vb, 101011-19-2; VIa, 101011-20-5; VIc, 101011-21-6; CO, 630-08-0; closed-$Fe_3(CO)_8(\mu_3\text{-}PPh)_2[PPh_3]^{-\cdot}$, 101011-22-7; open-$Fe_3(CO)_8(\mu_3\text{-}PPh)_2[PPh_3]^{-\cdot}$, 101011-24-9; open-$Fe_3(CO)_8(\mu_3\text{-}PPh)_2[P(OPh)_3]^{-\cdot}$, 101011-26-1; $P(OMe)_3$, 121-45-9; PEt_3, 554-70-1.

Supplementary Material Available: Tables of complete bond distances, bond angles, anisotropic thermal parameters, and structure factor amplitudes for the tris-phosphite IV (15 pages). Ordering information is given on any current masthead page.

Resonance Raman Spectroscopy of Metallochlorins. 2. Properties of Meso-Substituted Systems

Laura A. Andersson,[†] Thomas M. Loehr,*[†] Chariklia Sotiriou,[‡] Weishih Wu,[‡] and Chi K. Chang[‡]

Contribution from the Department of Chemical, Biological, and Environmental Sciences, Oregon Graduate Center, Beaverton, Oregon 97006-1999, and the Department of Chemistry, Michigan State University, East Lansing, Michigan 48824. *Received September 9, 1985*

Abstract: Nickel(II) and copper(II) complexes of meso-substituted chlorins (dihydroporphyrins) have been examined by FTIR and resonance Raman (RR) spectroscopy to determine whether their vibrational characteristics are in agreement with the observed properties of physiological chlorins (protoporphyrin IX-derived) recently reported by Andersson et al. (*J. Am. Chem. Soc.* **1985**, *107*, 182-191). The first red (647.1-nm) excitation spectra of a metallochlorin are presented, along with an excitation profile. The IR and RR spectra of nickel(II) *meso*-tetramethylchlorin (NiTMC) and copper(II) *meso*-tetraphenylchlorin (CuTPC) are considerably more complex than spectra of the analogous porphyrins. Despite the altered pattern of peripheral substituents in the meso-substituted metallochlorin systems, it is clear that a common set of vibrational properties is applicable to both meso-substituted and physiological metallochlorins: (a) an increase in the total number of RR bands; (b) an increase in the number of polarized RR bands; (c) the notable presence of one or more new polarized "chlorin" bands in the region of the oxidation-state marker; (d) altered polarization properties for B_{1g} and A_{2g} modes; (e) RR-active, split E_u (D_{4h} symmetry) modes; (f) predominance of polarized vibrational modes with both Soret and visible excitation; and (g) nearly identical frequencies in both IR and RR spectra. The observation that metallochlorin vibrational properties can be generalized extends the utility of such parameters to cover a wider variety of metallochlorins than has been studied to date and will aid in the understanding of metallochlorins both as model complexes and in biological systems such as the chlorophylls and/or the chlorin-containing green heme proteins.

Extensive investigations of biological and model metalloporphyrin systems by resonance Raman (RR) spectroscopy have established its utility as a probe of the characteristic molecular properties of these chromophores. This body of work, which has recently been reviewed,[1] includes identification of metalloporphyrin oxidation states and spin states, analysis of the effects of the central metal ion, examination of the influences arising from the type and number of axial ligands, assignment of low-frequency metal-ligand vibrations, assignment of vibrations arising from macrocyclic substituents (e.g., vinyl and formyl modes), and, where appropriate,

* To whom correspondence should be addressed.
[†] Oregon Graduate Center.
[‡] Michigan State University.

(1) Spiro, T. G. In *Iron Porphyrins, Part II*; Lever, A. B. P., Gray, H. B., Eds.; Addison-Wesley: Reading, MA, 1983; Chapter 3.

0002-7863/86/1508-2908$01.50/0